Unravelling the mechanisms of PFOS toxicity by combining morphological and transcriptomic analyses in zebrafish embryos

Rubén Martínez[1,2], Laia Navarro-Martín[1], Chiara Luccarelli[1], Anna E. Codina[3,4], Demetrio Raldúa[1], Carlos Barata[1], Romà Tauler[1], Benjamin Piña[1]*

[1]IDAEA-CSIC. Jordi Girona, 18. 08034 Barcelona, Spain

[2]Universitat de Barcelona (UB), Barcelona, 08007, Spain

[3]CNAG-CRG, Centre for Genomic Regulation (CRG), Barcelona Institute of Science and Technology (BIST), Barcelona, 08028, Spain

[4]Universitat Pompeu Fabra (UPF), Barcelona, 08003, Spain

Benjamin Piña (bpcbmc@cid.csic.es)

Rubén Martínez (rmlqam@cid.csic.es)

Laia Navarro-Martín (laianavarromartin@gmail.com)

Chiara Luccarelli (luccarellichiara@gmail.com)

Anna E. Codina (anna.esteve@cnag.crg.eu)

Demetrio Raldúa (drpqam@cid.csic.es)

Carlos Barata (cbmqam@cid.csic.es)

Romà Tauler (rtaqam@cid.csic.es)

* Corresponding author: Benjamin Piña, Institute of Environmental Assessment and Water Research, IDAEA-CSIC, Jordi Girona 18, 08034 Barcelona, Spain TEL. +34 93 4006100, ext 1551; E-mail: bpcbmc@cid.csic.es

*Graphical Abstract

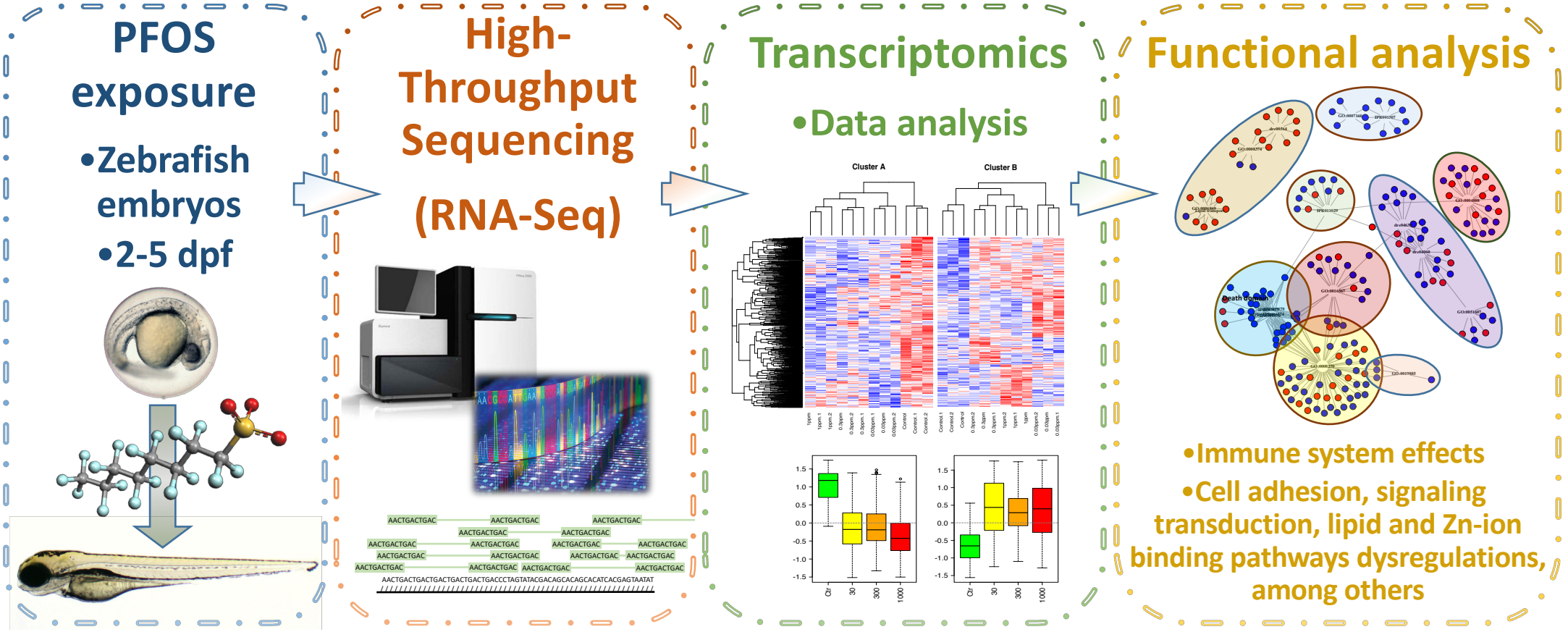

***Highlights (for review : 3 to 5 bullet points (maximum 85 characters including spaces per bullet point)**

Highlights

- Zebrafish embryos show macroscopic alterations at PFOS concentrations > 1mg/L
- Transcriptomic changes occur at concentrations 1/10 to 1/100 the macroscopic LOEC
- Transcript analyses suggest alterations on lipid metabolism and the immune system
- Some of the observed changes occur at concentrations already detected in humans
- We propose tighter regulations limiting human and environmental exposure to PFOS

Abstract

Exposure to PFOS (perfluorooctanesulfonate) has been related to toxic effects on lipid metabolism, immunological response, and different endocrine systems. We present here a transcriptomic analysis of zebrafish embryos exposed to different concentrations of PFOS (0.03-1.0 mg/L) from 48 to 120 hpf. No major survival or morphological alterations (swimming bladder inflation, kyphosis, eye separation and size...) were observed below the 1.0 mg/L mark. Conversely, we observed significant increase in transcripts related to lipid transport and metabolism even at the lowest used concentration. In addition, we observed a general decrease on transcripts related to natural immunity and defense again infections, which adds to the recent concerns about PFOS as immunotoxicant, particularly in humans. Derived PoD (Point of Departure) values for transcriptional changes (0.011 mg/L) were about 200-fold lower than the corresponding PoD values for morphometric effects (2.53 mg/L), and close to levels observed in human blood serum or bird eggs. Our data suggest that currently applicable tolerable levels of PFOS in commercial goods should be re-evaluated, taking into account its potential effects on lipid metabolism and the immune system.

Keywords: endocrine disrupting chemicals, high-throughput sequencing, differentially expressed genes (DEGs), ANOVA-PLS, immune system, lipid disruption, benchmark doses.

1. Introduction

Polyfluoroalkyl and perfluoroalkyl substances (PFASs) consist of fully fluorinated hydrophobic alkyl chains attached to different hydrophilic ending groups. Their unique thermal stability and oxidation resistance have fueled their use for more than 50 years in different industrial and domestic applications, as surfactants, surface treatment, fire retardants, and coating materials (OECD, 2002). However, these same properties make PFAS very bioaccumulative and persistent in the environment, with the capability for long range transport through the atmosphere and water (Ahrens and Bundschuh, 2014). Perfluorooctane sulfonate (PFOS) is one of the most frequently detected PFASs in the environment, and the first one to be added to Annex B of the Stockholm Convention on Persistent Organic Pollutants list, which resulted in a global restriction, but not a ban, on its production and use (Paul et al., 2009). Like other PFAS, exposure to PFOS is known to induce adverse effects on growth, birth weight, fertility, carcinogenesis, immunity, lipid metabolism, and the thyroid system (Chaparro-Ortega et al., 2018; Du et al., 2013; Jensen and Leffers; Lau, 2015). Nevertheless, neither PFOS nor any other PFAS has been yet categorized as endocrine disrupting chemical (EDC) by the European Commission (European Commission, 2000) or by other regulatory agencies. PFOS is found at relatively high levels (ng/L, µg/g and mg/L) in wastewaters, wastewater treatment plants' sludge, and exposed aquatic biota, respectively, showing an extremely high bioaccumulation potential (Ahrens and Bundschuh, 2014; Arvaniti and Stasinakis, 2015; Loos et al., 2013). In humans, blood serum levels of PFOS and other PFAS ranged from 1 to 10 µg/L in multiple surveys of general populations, and from 100 to 1000 µg/L for highly exposed populations (Kato et al., 2015; Olsen, 2015). Toxicological studies revealed potential toxic effects of these substances ranging from growth and reproductive functions to lipid metabolism and oxidative stress (Ankley et al., 2005; Lau et al., 2007; Rodriguez-Jorquera et al., 2019). The effect of the exposure to PFOS and other related compounds on the immunologic system is a matter of increasing concern, as it has been observed both in fish and in mammals, but its significance for human health is largely unknown (Corsini et al., 2011; DeWitt et al., 2009; DeWitt et al., 2016). Moreover, a recent report on the effect of PFOS on mice gut microbiome suggests an until now unexplored potentially harmful interactions between PFOS and microbial and animal metabolisms (Lai et al., 2018).

In the present study, we aimed to characterize and to describe the mechanisms of PFOS toxicity using zebrafish embryos as a model. Zebrafish characteristics (easy maintenance, small size, short life cycle, embryo transparency, large offspring, etc.) made it a preferred animal model for toxicity studies during the last decades (Hill et al., 2005; Scholz and Mayer, 2008; Stegeman et al., 2010). The study of zebrafish at least at genomic, transcriptomic, proteomic and metabolomic levels (Mushtaq et al., 2013) and its recognition as an acceptable vertebrate model for human and environmental toxicology (Raldúa and Piña, 2014; Strahle et al., 2012), make it an excellent election for ecotoxicological studies. During the last years, high-throughput next generation sequencing (HT-NGS) technologies facilitated the improvement and achievements of the transcriptomic studies (Mortazavi et al., 2008; Reuter et al., 2015), and showed its usefulness in the study of transcriptomic effects of several toxicants (Baker and Hardiman, 2014; Caballero-Gallardo et al., 2016). Although transcriptomics effects of PFOS over zebrafish larvae have been previously assessed, these studies were centered in a targeted dataset of transcripts (Jantzen et al., 2016; Shi et al., 2008) or based in a single PFOS dose (Chen et al., 2014; Fai Tse et al., 2016). The aim of this work was to analyze the toxic effects of PFOS in zebrafish embryos at sub-lethal concentrations, using a combination of morphometric and transcriptomic techniques. For that reason, we have designed dose-response assays using different PFOS concentrations to unravel the different mechanisms underlying the different toxic effects and to contribute to the risk assessment analysis of these currently ubiquitous pollutants.

2. Materials and methods

2.1. Zebrafish maintenance and rearing conditions

Adult wild-type zebrafish (*Danio rerio*, 12–18 months old) were maintained under controlled standard conditions (28 ± 1 °C, 12L:12D photoperiod, ≤ 5 fish/L) in fish water. Fish water was composed of 90 μg/ml of Instant Ocean (Aquarium Systems, Sarrebourg, France) and 0.58 mM of $CaSO_4 \cdot 2H_2O$, dissolved in reverse osmosis purified water. Zebrafish were fed twice a day with dry flakes (TetraMin, Tetra, Germany). Eggs were obtained by natural mating of the adults, placing in breeding tanks males and

females in a 2:1 proportion, respectively. A mesh was placed in each breeding tank to avoid zebrafish access to eggs, which were collected and rinsed at 2 hpf (hours post fertilization). Fertilization rate was assessed to be at least 70 % (OECD, 2013) and fertilized eggs were randomly placed in 6 well plates with fish water (under standard conditions) at a density of 3 embryos/mL. Fish water was changed daily until the start of the PFOS exposure at 48 hpf (**sections 2.2.2. and 2.2.3.**). All procedures were performed accordingly with the institutional guidelines under a license from the local government (DAMM 7669, 7964) and were approved by the Institutional Animal Care and Use Committees at the Research and Development Centre of the Spanish National Research Council (CID-CSIC).

2.2. Zebrafish eleutheroembryo exposure to PFOS

2.2.1. PFOS solutions preparation.

PFOS (perfluorooctanesulfonate (PFOS, CAS-RN: 2795-39-3) potassium salt) was purchased from Sigma-Aldrich (St. Louis, MO, USA, ≥98% purity). Five hundred-fold stock solutions (50-5000 mg/L, depending on the experiment, see sections 2.2.2. and 2.3.3.) were prepared in dimethyl sulfoxide (DMSO) and stored at -20 °C. Experimental solutions were prepared every day by dilution of the stock with fish water, with a final DMSO concentration of 0.2% (v/v) in all exposed and control groups. The pH of the working solutions was in the recommended range (6.8 - 7.5) (Avdesh et al., 2012). Concentrations are given as nominal values. Since the stability of PFOS in water solutions for at least 24h have been previously assessed (Kato et al., 2013; Lyu et al., 2015), daily water changes were considered sufficient to ensure constant PFOS concentrations.

2.2.2. Exposures for morphometric tests

Zebrafish eleutheroembryos were exposed from 2 dpf to 5 dpf to a wide range of PFOS concentrations to stablish a suitable LOAEC (Lowest Observed Adverse Effect Concentration) below which transcriptomics studies should take place. We did not expose embryos during the first 48 hpf to avoid confounding factors due to the interference of PFOS with the early embryonic processes and to focus in the effect of PFOS in the already differentiated tissues of the larvae. PFOS concentrations ranged

from 0 (control, 0.2% of DMSO) to PFOS solutions containing 0.10, 0.25, 0.50, 1.0, 2.5, 5.0, 7.5, 10 and 100 mg/L of PFOS (all of them in the presence of 0.2% of DMSO). Anatomical development of embryos was followed daily during the exposure as described (Kimmel et al., 1995) . Survival (3, 4 and 5 dpf), hatching (3, 4 and 5 dpf) and swim bladder inflation rates (4 and 5 dpf) were assessed in at least 50 larvae per each experimental group.

2.2.3. Exposure for transcriptome analysis

Using the morphometric data, a second round of PFOS exposure was performed, avoiding PFOS concentrations that could affect embryo viability. Therefore, the highest used concentration was 1.0 mg/L of PFOS, as determined as LOAEC for morphometric effects (**see section 3.2.**). Zebrafish eleutheroembryos were exposed to control (0.2% DMSO), 0.03, 0.3 and 1.0 mg/L of PFOS during 72h from 2 to 5 dpf. The experimental design was selected to minimize all possible covariates. All animals belonged to the same batch and were simultaneously incubated in 6-well plates, each one containing control and exposed groups for each concentration (no batch- or plate-bias). Fresh working solutions were daily prepared from the stocks and renewed as previously described. For each experimental group, anatomical development of embryos (Kimmel et al., 1995), sub-lethal and developmental efects, survival and hatching rates at 3, 4 and 5 dpf, and swim bladder inflation rates at 4 and 5 dpf were reported, according to the OECD 236 guidelines (OECD, 2013). Replicates of 10 eleutheroembryos per experimental condition were collected, snap-frozen in dry ice and stored at -80 °C until further analysis (RNA extraction for high-throughput sequencing and RT-qPCR confirmation purposes).

2. 3. Eleutheroembryo fixation, morphological and immunochemical measurements

Zebrafish eleutheroembryos were collected and fixed overnight at 4 °C in a phosphate buffered saline 1X solution (PBS) with 4% PFA (paraformaldehyde) as previously described (Martínez et al., 2018; Raldua et al., 2008). For morphological measurements, fixed eleutheroembryos were then washed several times with PBS and gradually transferred to 90% glycerol (10% PBS 1X) for long-term preservation and positioning facilitation under the microscope. A stereomicroscope Nikon SMZ1500

equipped with a Nikon digital Sight DS-Ri1 camera was used to acquire lateral and dorsoventral images of the fixed embryos (**Figure 1A**). Afterwards the following morphological parameters were measured using the free graphical image analysis software ImageJ (National Institutes of Health, Bethesda, MD, USA): Body length (BL), head-trunk angle (HTA), yolk sac area (YSA), swim bladder area (SBA), eye length (EL), eye width (EW), head width (HW), inter-ocular distance (IOD) and eye-snout distance (ESD) (**Figure 1C**). For immunochemical determinations, fixed eleutheroembryos were washed several times with PBS, gradually transferred to methanol 100 %, and stored at -80 °C for at least 24h. After rehydration of the larvae, a 50 min depigmentation step (3% H_2O_2 and 1% KOH in water) was included before the permeabilization steps. Whole mount immunohistochemistry was performed as previously described with minor modifications (Thienpont et al., 2011). Larvae were then incubated overnight at 4 °C in either anti-parvalbumin monoclonal antibody (Sigma-Aldrich, St. Louis, MO) at 1:2000 and anti-acetylated alpha-tubulin monoclonal antibody (Sigma-Aldrich, St. Louis, MO) at 1:1000. The above primary antibodies were used to detect ciliated and microvillous olfactory sensory neurons (anti-parvalbumin, *Parv*) and cilia from olfactory epithelium and neuromast hair cells (acetylated alpha-tubulin, *α-AT*), respectively. The secondary antibodies used were Alexa Fluor 488 and 555 goat anti-rabbit IgG and goat anti-mouse IgG (1:300; Molecular Probes).

2.4. RNA extraction, library construction and high-throughput sequencing

Total RNA was isolated from independent pools of 10 eleutheroembryos (three pools for each condition, separately exposed and treated) using AllPrep DNA/RNA Mini Kit (Qiagen, CA, USA) as described by the manufacturer. Extracted RNA was reconstituted in RNAse-free water and its quantity and quality were determined by a Qubit® RNA BR Assay kit (Thermo Fisher Scientific) and RNA 6000 Nano Assay on a Bioanalyzer 2100 (Agilent Technologies), respectively. RNA preparations were sent to the National Center for Genomic Analysis (CNAG, Barcelona, Spain) for high-throughput sequencing (RNA-Seq). All replicates showed RNA concentrations between 50 and 200 ng/µL, were free of genomic DNA and had an RNA integrity number (RIN) > 8. The RNA-Seq libraries were prepared using KAPA Stranded mRNA-Seq Kit Illumina® Platforms (Kapa Biosystems) with minor modifications. A poly-A based mRNA

enrichment with oligo-dT magnetic beads was performed over 500 ng of total RNA as input material. The mRNA was fragmented (resulting RNA fragment size: 80-250nt; major peak: 130nt). The second strand cDNA synthesis was carried out in the presence of dUTP instead of dTTP, to enhance strand specificity. The blunt-ended double-stranded cDNA was 3´ adenylated and Illumina indexed adapters (Illumina) were ligated. Ligation product was enriched with 15 PCR cycles and validated on an Agilent 2100 Bioanalyzer with the DNA 7500 kit. Each final library was sequenced using TruSeq SBS Kit v3-HS (paired-end mode; 2x76bp as read length). An average of 39 million paired-end reads for each sample was generated in a fraction of a sequencing lane on HiSeq 2000 (Illumina). Image analysis, base calling and quality scoring of the run were processed using the manufacturer's software Real Time Analysis (RTA 1.13.48) and FASTQ sequence files were generated by the sequencing analysis software CASAVA. Obtained reads mapped properly to the reference genome in more than a 95%. The majority mapped to exonic regions and to protein-coding genes, with a total of 24,425 genes detected. The transcriptomic data discussed in this publication have been deposited in NCBI's Gene Expression Omnibus (Edgar et al., 2002) and are accessible through GEO Series accession number GSE125072 (https://www.ncbi.nlm.nih.gov/geo/query/acc.cgi?acc=GSE125072). A full description of mapping quality statistics can be found in **Supplementary Table ST1**.

2.5. Data analysis

2.5.1. Morphometric statistical analysis

Differences between experimental groups in survival, hatching and swim bladder inflation rates (**sections 2.2.2. and 2.2.3.**) and morphological measurements (**section 2.3.**) were analyzed by non-parametric Kruskal-Wallis tests plus Dunn's pairwise multiple comparisons (significance level at $p < 0.05$, Bonferroni correction). SPSS 24.0 (Armonk, NY: IBM Corp., 2016) was used to carry out statistical tests whereas GraphPad Prism (v. 6.07, GraphPad Software, La Jolla, CA, USA) was used to perform the graphs (**Figure 1C and Supplementary Figures SF1, SF2, SF3**).

2.5.2. RNA-Seq data analysis

RNA-Seq reads were aligned to the *D. rerio* reference genome (GRCz10) using the STAR software version 2.5.1b (Dobin et al., 2013). The quantification of the genes annotated in GRCz10.84 were performed using RSEM version 1.2.28 (Li and Dewey, 2011) with default parameters. Data normalization was carried out using the DESeq2 (v.1.10.1) R package (Li and Dewey, 2011; Love et al., 2014), which uses a variant of scaling factor normalization based on the assumption that most genes are not differentially expressed. Differential expression analysis between all experimental conditions was analyzed using the ANOVA-PLS (Analysis of Variance-Partial Least Square) analysis using the *lmdme* package in R v. 1.0.136, R Core Team (Fresno et al., 2014). First, ANOVA decomposed the transcriptomic data matrix of all samples (normalized and scaled) through a linear model that considers the experimental design (PFOS treatment). Secondly, a PLS regression model was built between the matrices obtained in this linear decomposition (X) and a vector (y) that defined the class membership of the samples (control, 0.03, 0.3 and 1.0 mg/L). The analysis identified the features (variables) that described best the differences between groups and it determined if the experimental groups were different from each other. ANOVA-PLS was performed on the normalized data scaled to the control set and log2 transformed, considering each one of the PFOS concentrations (including controls) as a class. Genes showing significant variations among the classes ($p \leq 0.05$; 1434 transcripts in total) were selected as DEGs (differentially expressed genes) for further analysis. Hierarchical and PAM (partition around medoids) clustering analysis were performed using the packages *gplots*, *fpc*, and *cluster* in R. The PAM implementation in these packages allowed performing a principal components analysis (PCA) to analyze the covariance matrix of the entered variables and to produce a 2D plot showing the goodness of separation of the defined clusters (https://www.rdocumentation.org/packages/cluster/versions/2.0.6/topics/pam). Statistically significant differences between genes included in each cluster were assessed by one-way ANOVA followed by post hoc Tukey's B tests ($p < 0.05$) using the *foreign* and *agricolae* packages in R. Further graphs were carried out using the *gplots* package, also in R environment. DAVID Bioinformatic Resources 6.8 was used for the functional analysis of DEGs. Gene enrichment analysis was estimated in DAVID using the default zebrafish background setting the enrichment significances to a false

discovery ratio (FDR) ≤ 5%. Identified modules with at least four hits were included in the network analysis, using the *reshape2* and *igraph* packages in R (R_Development_Core_Team, 2008). Graphs were elaborated from an incidence table of genes (represented by their official gene names, ZFIN.org) using the *igraph* package. Any two given genes were considered linked if they shared at least one common KEGG or GO (Gene Ontology) module. Metabolic pathways were obtained from the KEGG (Kyoto Encyclopedia of Genes and Genomes) database.

2.5.3. Benchmark dose and point of departure determination

Benchmark doses (BMD) for both morphometric and RNAseq data were calculated using the BMDExpress 2.2 sofware (https://www.sciome.com/bmdexpress/)(Phillips et al., 2018; Yang et al., 2007). Benchmark dose lower confidence limits (BMDLs) were calculated to stablish a reference dose or point of departure (PoD) for both datasets (Bhat et al., 2013; EPA, 2012; Farmahin et al., 2017; Webster et al., 2015).

3. Results and Discussion

3.1 Survival and morphometric analyses

No statistically significant differences (non-parametric Kruskal-Wallis test, $p > 0.05$) were observed in hatching rates at PFOS concentrations up to 100 mg/L (**Supplementary Figure SF1A**). On the other hand, we observed a significant increase in mortality rates at 5 dpf when embryos were exposed to 7.5, 10 and 100 mg/L and estimated LC50 at 9.1 mg/L. Swim bladder inflation was reduced at PFOS concentrations equal or higher than 2.5 mg/L, at both 4 and 5 dpf. Other lethal endpoints such as lack of heartbeat, coagulated embryos, lack of somite formation, or non-detachment of the tail, were not observed.

Several sublethal morphological changes, like appearance of spinal deformities (bent spine) and scoliosis, reduction of body length (BL), reduction of eye-snout distance (ESD), decrease in swim bladder area (SBA) or increases in yolk sac area (YSA) were observed at 5 dpf at PFOs concentrations equal or higher than 5 mg/L (Figures 1 A-C, **Supplementary Table ST2**). This result was in concordance with previous reports of skeletal deformations (scoliosis and kyphosis) induced by PFOS and other

perfluorinated compounds in zebrafish embryos (Hagenaars et al., 2014). Other quantitative morphological parameters, like eye and head width (EW and HW, respectively) and inter-ocular distance (IOD), were reduced respect to the controls at concentrations equal or higher than 2.5 mg/L of PFOS (6-15%, 9-20% and 15-35% respectively, **Figures 1 B, C**), whereas reductions of the head-trunk angle (HTA) and eye length (EL) showed some significant variations at the 1 mg/L of PFOS concentration (**Figures 1 B, C**). Note that morphological parameters could not be determined at the highest concentrations (10 and 100 mg/L) due to their high rates of mortality (82 and 100 %, respectively). Using the BMDExpress software we calculated PFOS BMDLs for all measured morphological features and found HTA and YSA as the most and less affected parameters, respectively ($BMDL_{HTA}$ = 1.27 mg/L, $BMDL_{YSA}$ = 5.78 mg/L). Taking this into account, we used the median BMDL of all morphological features to estimate 2.53 mg/L of PFOS as the morphologic point of departure (PoD) for our study. These results were consistent with previously reported LOAEC values of 1.0 mg/L for activity/behavior (Spulber et al., 2014), 1.0-2.0 mg/L for morphometric alterations (Hagenaars et al., 2014; Shi et al., 2008) or 1.66 mg/L for PFOS ototoxicity (Stengel et al., 2017). We also tested effects on olfactory epithelium and lateral line neuromasts, since they are considered as sensitive markers for neurotoxic or cytotoxic effects of PFOS and other toxicants in zebrafish (Chen and Reese, 2013; de Esch et al., 2012; EPA, 2018; Hirose et al., 2011; Sato et al., 2009). Using immunochemical techniques, we observed no evident effects on the olfactory epithelium or on lateral line neuromasts at PFOS concentrations up to 1.0 mg/L, indicating lack of neurotoxicity at this PFOS concentration range (**Figure 1D)**. Taking into consideration all the above exposed reasons, we selected 1.0 mg/L as the maximum PFOS concentration used for the exposures in the transcriptomic study.

3.2 Transcriptome analyses

The ANOVA-PLS analysis identified 1434 transcripts as DEGs in at least one of the exposure groups with respect to the others. Hierarchical clustering of DEGs showed that the expression profiles of the selected DEGs closely reflected the experimental setup, as the different biological replicates for all treatment groups fell into the same hierarchical cluster (**Figure 2A**, note that the white cells corresponds to

the averaged control levels and red and blue cells, correspond to over- and under-expressed transcripts, respectively). Unexposed control samples appeared as a clearly differentiated group from the exposed ones. PAM clustering confirmed this rather gradual dose-response pattern by defining two clusters, A and B, corresponding to genes whose abundances decreased (767 genes) or increased (667 genes) upon PFOS exposure, respectively (**Figure 2 B-D**). Note that the samples of each exposure group clustered together in both clusters. Cluster A showed a clear separation between control and exposed samples, whereas the two highest doses (0.30 and 1.0 mg/L) separated from the 0.03 mg/L group. Cluster B shows a slightly different grouping of samples, as controls and the low dose (0.03 mg/L) clustered separately from the 0.30 and 1.0 mg/L groups. **Figure 2D** shows the distribution of normalized expression values (mean = 0, standard deviation = 1) for all genes in both clusters and reflects the higher difference in the under-expression of the genes (cluster A) between non-treated (control) and treated samples than those among the different dose groups. The dose-response pattern is less evident in cluster B. We thus conclude that the LOAEC for transcriptomic effects of PFOS (at least, for the major part of it) is likely below 0.03 mg/L (30 ppb), as these samples separated themselves from controls. Moreover, we estimated 0.011 mg/L of PFOS (11 ppb) as PFOS transcriptomic PoD, about a third of the lowest concentration used in the transcriptomic study (**Supplementary Figure SF1B**). This is more than 200 fold lower than the estimated PoD value for morphometric changes (**Supplementary Figure SF1B**), and lower than the reported limit of detection for transcriptomic effects of PFOS by targeted analyses (0.10 mg/L, (Jantzen et al., 2016; Shi et al., 2008). RNA-seq transcriptomic data exposed in this study was confirmed by RT-qPCR (**Supplementary Methods, Supplementary Figure SF2, Supplementary Table ST3**) showing a strong correlation between both techniques in several selected genes ($r^2 = 0.814$, $p < 10^{-4}$).

3.3 Functional analysis

DAVID functional analysis showed a relatively small subset of functional classes significantly enriched either in any of the two clusters or in the whole DEGs subset (**Table 1**, see also **Figure 3A and supplementary Table ST4**). Particularly notable is the case for over-represented transcripts (Cluster B), in which all significantly enriched

functional classes were related to lipid transport and/or metabolism (**Table 1**). This is consistent with the known disruption of lipid homeostasis by PFOS and other structurally-related compounds in vertebrates (Das et al., 2017; Huang et al., 2016), and it shows a similar pattern as the lipid metabolism/transport transcriptomic effects induced by other EDCs like Bisphenol A (Martínez et al., 2018) (**Supplementary Figure SF3**, $r^2 = 0.678$, $p < 10^{-4}$). The presence of yolk sac remains observed in the present study (**section 3.2.**) is also in agreement with the alterations in the lipid homeostasis shown at the transcriptomic level.

Several functional modules associated to Cluster A were identified by DAVID analysis, although most of them corresponded to structural, rather than functional categories (**Table 1**, **Figure 3A**). For example, the observed transcriptomic dysregulations in myosin, actin and tropomyosin transcripts (**Supplementary figure SF4**) are in agreement with the observed spinal deformities (**section 3.2.**), which have been in turn related to alterations in myosin and other muscle fibers (Huang et al., 2010). As it can be observed in **Supplementary figure SF4**, genes in cluster A exhibited a classic dose-response pattern, increasing their expression according to the PFOS exposure. Nevertheless, the relationship between the dysregulation of these genes and the effects on the spinal cord and tail structure need to be confirmed by a further specific research.

Most enriched functional categories in Cluster A (KEGG or GO_BP terms) appeared related to the immunological system and/or pathogen response, including several cytokines, cytokine signaling-related proteins, proteases implicated to antigen presentation, or the JAK-STAT signaling pathway (**Table 1**). This is consistent with the known dysregulation of the immune system caused by PFOS and other perfluorinated substances, which includes changes in cytokines production (DeWitt et al., 2009; Lau et al., 2007; Peden-Adams et al., 2008; Suo et al., 2017). Structurally-defined modules (INTERPRO or GO_MF terms in **Table 1**) included a relatively large group of genes associated to the structural domain B30.2/SPRY and Zn-ion binding proteins, among others. While the structural domain B30.2/SPRY have been reported to be involved in immunity and immunoglobulins (D'Cruz et al., 2013; Howe et al., 2016; Woo et al., 2006), zinc fingers (structural motif of the proteins which Zn binds to) have an extraordinary diversity of both structures and functions (Kluska et al., 2018; Laity et al.,

2001).

Considering the whole DEG dataset, more general functions appear, including signaling, extracellular space and transmembrane receptor activity. Inspection of the genes identified by their structural, rather than functional characteristics, revealed the biological processes potentially affected by their de-regulation. These interdependences can be visualized in the network shown in **Figure 3B**. For example, the structural class "IPR001507: Zona pellucida domain" shares some genes with the functional class "cell-matrix adhesion" (both in cluster A), suggesting alterations in cell-cell interactions. Similarly, the structural class "IPR011029: Death-like domain" may be related to programmed cell-death pathways, as most of the 13 genes identified as DEGs are also related to caspase recruitment, apoptosis, or TNF (tumor necrosis factor) activation (**Table 1**). This is consistent with previous studies in cells (Cui et al., 2017; Shi et al., 2008; Zhang et al., 2013) and zebrafish (Shi et al., 2008). Particularly noticeable is the structural-based module "IPR001870:B30.2/SPRY domain" that, together with closely-related structural terms (IPR003879 and IPR013320, among others), includes many components of the so-called TRIM protein family, a group of E3-ligase proteins functionally related to the innate immunity development (Versteeg et al., 2013) (**Table 1**). Most detected members of this family corresponded to the fish-specific finTRIM subfamily (FTR genes, **Table 1**), also putatively related to different aspects of the fish immune response (van der Aa et al., 2012). Also members of the TRIM family are the *bloodthirsty* (*btr*) genes, orthologous to the human TRIM39 protein and also potentially related with the above mentioned immune response (Luo et al., 2017; van der Aa et al., 2012; Zhang et al., 2015). All these genes appeared as down-regulated by the exposure to PFOS (**Figure 3**, note that they are placed in cluster A).

Cell adhesion, another of the affected pathways in our study, is mediated by four major protein superfamilies (immunoglobulins, selectins, cadherins and integrins; a.k.a. CAMs). Immunoglobulins and selectins are involved in the immune response (Mashoof and Criscitiello, 2016; Roca et al., 2008; Sun et al., 2015); cadherins in the actin fibers linkeage through catenins (Li-Villarreal et al., 2016); and integrins facilitate the extracellular matrix adhesion, also activating the signaling transduction pathways including the apoptosis signals, among others (Mould et al., 2006). We observed that all those pathways were transcriptionally affected by PFOS (**Table1, Figure 3**). Although

the data suggests the existence of a PFOS-induced initial toxic event related to cell adhesion and/or the signaling pathways, further studies are required in order to achieve a deeper comprehension about its mode of action.

It is remarkable how interweaved were the observed transcriptomics effects with themselves and with the phenotypic alterations, suggesting a common initial triggering point. For example, the structural and functional diversity of lectins (the above mentioned IPR013320 structural term is a subgroup of them) have been previously studied in teleost fish, showing their involvement not only in the immune response (Vasta et al., 2011), but also in lipid regulation (Cambi et al., 2005; Ng et al., 1989), and that lectin malfunction may result in bent tails and other skeletal muscle problems in zebrafish (Ahmed et al., 2009), which are similar to the ones observed in our exposed animals.

3.4 Toxicological relevance

Many animal and in vitro human systems indicate that exposure to PFOS may result in neurotoxicity, immunotoxicity, thyroid disruption, reproductive, cardiovascular and pulmonary toxicity, and diverse toxic effects in liver and kidneys (Das et al., 2017; DeWitt et al., 2009; Lau et al., 2007; Suo et al., 2017; Zeng et al., 2019). These studies suggest that PFOS represent a significant hazard for human health. This has been at least partially confirmed by the still scarce epidemiological studies, being water and food the two main sources of exposure (Zeng et al., 2019). In addition to their implication for human health, the wide use, high persistence, and bioaccumulative properties of PFOS and other PFAS implicate that they are ubiquitous in the environment, and in particular, in aquatic bodies. PFOS and other PFAS has been detected in fish and marine mammal and bird tissues at ng-µg/g ww levels (Ahrens and Bundschuh, 2014; Giesy and Kannan, 2001; Houde et al., 2011; Lau et al., 2007; Rodriguez-Jorquera et al., 2016). Both molecular and macroscopic effects have been reported for PFOS and other perfluoroorganic compounds in zebrafish embryos and adults (Chen et al., 2013; Cui et al., 2017; Fai Tse et al., 2016; Hagenaars et al., 2014; Lau et al., 2007; Shi et al., 2009). Similar effects have been reported in fathead minnows (*Pimephales promelas*) exposed to urban wastewaters presenting from ng to

μg/L levels of different PFAS (Rodriguez-Jorquera et al., 2015). In addition, there is a growing evidence of toxic effects of perflouroorganic compounds in invertebrates and plants (Giesy et al., 2010; Li, 2009; Stylianou et al., 2019).Therefore, we consider that our findings reflect toxic effects relevant not only for human health, but also for the environment.

Lipid metabolism, immunological response and transmembrane/intracellular signaling appeared as the main cellular functions affected by PFOS exposure at the molecular level (Das et al., 2017; DeWitt et al., 2009; Lau et al., 2007; Suo et al., 2017). The favorite mechanism of action (MoA) proposed for PFOS toxicity involves its interaction with nuclear receptors intimately involved in metabolic regulation and immunological functions, like PPARα (peroxisome proliferator activating receptor), CAR (constitutive androstane receptor), PXR (pregnane X receptor) or FXR (farnesoid X receptor) (Lau et al., 2007; White et al., 2011). While our experimental approach does not allow the characterization of the molecular mechanisms underlying the observed changes, they are essentially consistent with this MoA, which explain the simultaneous deregulation of genes involved in lipid metabolism and immuno response, among others. The effect of PFOS on lipid metabolism (including glycerophospholipids) of zebrafish embryos was also observed at the metabolic level (Ortiz-Villanueva et al., 2018), and it is likely related to the observed changes in yolk sac absorption. Therefore, our data show essentially the same kind of responses at gene expression, metabolism and morphological level.

PFOS is usually found at low levels (in the range of ng/L) in surface waters (Kunacheva et al., 2011; Vedagiri et al., 2018), particularly those under the influence of sewage treatment plants (Rodriguez-Jorquera et al., 2015; Rodriguez-Jorquera et al., 2016). However, PFOS is considered a persistent pollutant and its high bioaccumulation and low elimination rates (Huang et al., 2010; Kannan et al., 2005) cause PFOS to be found at very high levels (0.05-5.0 mg/kg) in wildlife (Hoff et al., 2005). It has been reported a 10-fold bioaccumulation between the water and exposed-whole zebrafish larvae tissues in only 5 days of PFOS exposure (Huang et al., 2010). Our PoD values for PFOS estimated from either morphometric (2.53 mg/L) or transcriptional data (0.011 mg/L) were higher than the environmental limits established for drinking water (10^{-5}-10^{-4} mg/L) according to both EPA and EFSA, as well

as other regulatory agencies (EC, 2004; Grandjean, 2018). Nevertheless, exposure routes for PFOS are diverse, and there are considerably higher legal limits for some purposes, like the 10 mg/kg limit for substances and preparations in the EU (EC, 2004). Regarding internal exposure levels, several studies have observed concentrations from 0.002 mg/L to 0.080 mg/L of PFOS in human serum of individuals from Asia, North America and Europe (Alexander et al., 2008; Jin et al., 2007; Vedagiri et al., 2018; Zeng et al., 2015) and even higher concentrations (0.145-0.381 mg/kg) in fish eggs (Kannan et al., 2005). This indicates that both humans and wildlife may be exposed to PFOS concentrations similar to or even higher than our calculated transcriptomic PoD value. Barring the need for dose-conversion and pharmacokinetics modeling to extrapolate the effects in zebrafish to humans, our results supported a very low safety margin, as they could imply that the immune system of exposed individuals, among others systems, could be affected at least at the transcriptomic level. In this regard, the suppression of immunological responses by different pollutants has been largely neglected until very recently, partially because the lack of an appropriate animal or cell models for its toxicological assessment (Möller et al., 2014; Rehberger et al., 2017; Segner et al., 2017). However, there is an increasing amount of evidence that some pollutants may indeed decrease the ability of fish and other vertebrates to fend off challenging infections (Fang et al., 2013; Quesada-Garcia et al., 2016). In the same direction, a report from the USA National Toxicology program also identified immunotoxicity as an emerging adverse effect of perfluorinated substances in humans (NPT, 2016). For all those reasons, we propose the inclusion of immunotoxicity tests in the existing zebrafish embryo testing schemes, which currently cover cardiovascular, nervous, neuromuscular, gastrointestinal and thyroid systems (Raldúa and Piña, 2014), to assess toxic effects of different substances in humans and other vertebrates.

4. Conclusions

Our results suggest a complex, multiple endocrine disruption-like toxic effects at concentrations well below the LOAEC/NOAEC for many of the macroscopic effects traditionally linked to PFOS toxicity in zebrafish embryos. While our results confirm the known effect of PFOS in the spinal cord, and its potential role as lipid disruptor, we found a significant decrease in the expression of many genes related to natural

immunity and defense against infections, previously reported in other organisms. Therefore, we suggest that a common initial key event may trigger all observed adverse effects elicited by exposure to PFOS. We propose that the transcriptional pattern may be a marker for the immunotoxic effects of PFOS and other related substances in fish and other vertebrates, including humans. As the estimated PoD values for transcriptional changes occurred at concentrations already found in living organisms, including humans, our data suggest that current maximal tolerable levels may not protect adequately environmental and human health and might need to be revised.

Conflicts of interest

The authors declare that they have no conflicts of interest.

Acknowledgements

This work was supported by European Union's Seventh Framework Programme (FP/2007-2013)/ERC Grant Agreement n. 320737, and by the Spanish Ministry of Economy and Competitiveness (CTM2014-51985-R). AEC acknowledges the funding from ISCIII (Spanish Ministry of Economy and Competitiveness, grant number PT17/0009/0019), co-financed by the European Fund for Regional Development (FEDER). LNM was supported by a Beatriu de Pinos Postdoctoral Fellowship (2013BP-B-00088) funded by the Secretary for Universities and Research of the Department of Economy and Knowledge of the Government of Catalonia and the Cofund programme of the Marie Curie Actions of the 7th R&D Framework Programme of the European Union. RML was supported by an FPU Fellowship (FPU15/03332) from the Spanish Ministry of Education, Culture and Sport.

References

555 Ahmed, H., Du, S.J., Vasta, G.R., 2009. Knockdown of a galectin-1-like protein in
556 zebrafish (Danio rerio) causes defects in skeletal muscle development, 3 ed, pp. 277-
557 283.
558 Ahrens, L., Bundschuh, M., 2014. Fate and effects of poly- and perfluoroalkyl
559 substances in the aquatic environment: A review. Environmental Toxicology and
560 Chemistry 33, 1921-1929.
561 Alexander, J., Atli Auðunsson, G., Benford, D., Cockburn, A., Cravedi, J.-P., Dogliotti, E.,
562 Di Domenico, A., Luisa Fernández-Cruz, M., Fink-Gremmels, J., Fürst, P., Galli, C.,
563 Grandjean, P., Gzyl, J., Heinemeyer, G., Johansson, N., Mutti, A., Schlatter, J., van
564 Leeuwen, R., van Peteghem, C., Verger, P., 2008. Perfluorooctane sulfonate (PFOS),
565 perfluorooctanoic acid (PFOA) and their salts Scientific Opinion of the Panel on
566 Contaminants in the Food chain. Efsa Journal 6, 1-131.
567 Ankley, G.T., Kuehl, D.W., Kahl, M.D., Jensen, K.M., Linnum, A., Leino, R.L., Villeneuve,
568 D.A., 2005. Reproductive and developmental toxicity and bioconcentration of
569 perfluorooctanesulfonate in a partial life-cycle test with the fathead minnow
570 (Pimephales promelas). Environmental Toxicology and Chemistry 24, 2316-2324.
571 Arvaniti, O.S., Stasinakis, A.S., 2015. Review on the occurrence, fate and removal of
572 perfluorinated compounds during wastewater treatment. Science of the Total
573 Environment 524, 81-92.
574 Avdesh, A., Chen, M., Martin-Iverson, M.T., Mondal, A., Ong, D., Rainey-Smith, S.,
575 Taddei, K., Lardelli, M., Groth, D.M., Verdile, G., Martins, R.N., 2012. Regular Care and
576 Maintenance of a Zebrafish (Danio rerio) Laboratory: An Introduction.
577 Journal of Visualized Experiments, e4196-e4196.
578 Baker, M.E., Hardiman, G., 2014. Transcriptional analysis of endocrine disruption using
579 zebrafish and massively parallel sequencing. Journal of Molecular Endocrinology 52,
580 R241-256.
581 Bhat, V.S., Hester, S.D., Nesnow, S., Eastmond, D.A., 2013. Concordance of
582 Transcriptional and Apical Benchmark Dose Levels for Conazole-Induced Liver Effects in
583 Mice. Toxicological Sciences 136, 205-215.
584 Caballero-Gallardo, K., Olivero-Verbel, J., Freeman, J.L., 2016. Toxicogenomics to
585 evaluate endocrine disrupting effects of environmental chemicals using the zebrafish
586 model. Current genomics 17, 515-527.
587 Cambi, A., Koopman, M., Figdor, C.G., 2005. How C-type lectins detect pathogens, pp.
588 481-488.
589 Chaparro-Ortega, A., Betancourt, M., Rosas, P., Vázquez-Cuevas, F.G., Chavira, R.,
590 Bonilla, E., Casas, E., Ducolomb, Y., 2018. Endocrine disruptor effect of perfluorooctane
591 sulfonic acid (PFOS) and perfluorooctanoic acid (PFOA) on porcine ovarian cell
592 steroidogenesis. Toxicology in Vitro 46, 86-93.
593 Chen, J., Das, S.R., La Du, J., Corvi, M.M., Bai, C., Chen, Y., Liu, X., Zhu, G., Tanguay, R.L.,
594 Dong, Q., Huang, C., 2013. Chronic PFOS exposures induce life stage-specific behavioral
595 deficits in adult zebrafish and produce malformation and behavioral deficits in F1
596 offspring. Environmental Toxicology and Chemistry 32, 201-206.
597 Chen, J., Tanguay, R.L., Tal, T.L., Gai, Z., Ma, X., Bai, C., Tilton, S.C., Jin, D., Yang, D.,
598 Huang, C., Dong, Q., 2014. Early life perfluorooctanesulphonic acid (PFOS) exposure
599 impairs zebrafish organogenesis. Aquatic Toxicology 150, 124-132.

Chen, Y., Reese, D.H., 2013. A Screen for Disruptors of the Retinol (Vitamin A) Signaling Pathway. Birth Defects Research Part B-Developmental and Reproductive Toxicology 98, 276-282.
Corsini, E., Avogadro, A., Galbiati, V., dell'Agli, M., Marinovich, M., Galli, C.L., Germolec, D.R., 2011. In vitro evaluation of the immunotoxic potential of perfluorinated compounds (PFCs). Toxicology and Applied Pharmacology 250, 108-116.
Cui, Y., Lv, S., Liu, J., Nie, S., Chen, J., Dong, Q., Huang, C., Yang, D., 2017. Chronic perfluorooctanesulfonic acid exposure disrupts lipid metabolism in zebrafish. Human & Experimental Toxicology 36, 207-217.
D'Cruz, A.A., Babon, J.J., Norton, R.S., Nicola, N.A., Nicholson, S.E., 2013. Structure and function of the SPRY/B30.2 domain proteins involved in innate immunity. Wiley-Blackwell, pp. 1-10.
Das, K.P., Wood, C.R., Lin, M.T., Starkov, A.A., Lau, C., Wallace, K.B., Corton, J.C., Abbott, B.D., 2017. Perfluoroalkyl acids-induced liver steatosis: Effects on genes controlling lipid homeostasis. Toxicology 378, 37-52.
de Esch, C., Slieker, R., Wolterbeek, A., Woutersen, R., de Groot, D., 2012. Zebrafish as potential model for developmental neurotoxicity testing: a mini review. Neurotoxicology and Teratology 34, 545-553.
DeWitt, J.C., Shnyra, A., Badr, M.Z., Loveless, S.E., Hoban, D., Frame, S.R., Cunard, R., Anderson, S.E., Meade, B.J., Peden-Adams, M.M., Luebke, R.W., Luster, M.I., 2009. Immunotoxicity of perfluorooctanoic acid and perfluorooctane sulfonate and the role of peroxisome proliferator-activated receptor alpha, pp. 76-94.
DeWitt, J.C., Williams, W.C., Creech, N.J., Luebke, R.W., 2016. Suppression of antigen-specific antibody responses in mice exposed to perfluorooctanoic acid: Role of PPAR alpha and T- and B-cell targeting. Journal of Immunotoxicology 13, 38-45.
Dobin, A., Davis, C.A., Schlesinger, F., Drenkow, J., Zaleski, C., Jha, S., Batut, P., Chaisson, M., Gingeras, T.R., 2013. STAR: Ultrafast universal RNA-seq aligner. Bioinformatics 29, 15-21.
Du, G., Hu, J., Huang, H., Qin, Y., Han, X., Wu, D., Song, L., Xia, Y., Wang, X., 2013. Perfluorooctane sulfonate (PFOS) affects hormone receptor activity, steroidogenesis, and expression of endocrine-related genes in vitro and in vivo. Environmental Toxicology and Chemistry 32, 353-360.
EC, 2004. Regulation (EC) No 850/2004 of the European Parliament and of the Council of 29 April 2004 on persistent organic pollutants and amending Directive 79/117/EEC, in: Council, E.P.a. (Ed.). European Commission, Brussels (Belgium).
Edgar, R., Domrachev, M., Lash, A.E., 2002. Gene Expression Omnibus: NCBI gene expression and hybridization array data repository. Nucleic Acids Res 30, 207-210.
EPA, R.A.F., 2012. Benchmark Dose Technical Guidance, in: Agency, U.E.P. (Ed.), EPA/100/R-12/001. EPA, Washington, D.C.
EPA, R.A.F., 2018. Exposure to PFOS, PFHxS, or PFHxA, but not GenX, Nafion BP1, or ADONA, elicits developmental neurotoxicity in larval zebrafish, in: Agency, U.S.E.P. (Ed.).
European Commission, D.E., 2000. Towards the establishment of a priority list of substances for further evaluation of their role in endocrine disruption.
Fai Tse, W.K., Li, J.W., Kwan Tse, A.C., Chan, T.F., Hin Ho, J.C., Sun Wu, R.S., Chu Wong, C.K., Lai, K.P., 2016. Fatty liver disease induced by perfluorooctane sulfonate: Novel insight from transcriptome analysis. Chemosphere 159, 166-177.

Fang, C., Huang, Q.S., Ye, T., Chen, Y.J., Liu, L.P., Kang, M., Lin, Y., Shen, H.Q., Dong, S.J., 2013. Embryonic exposure to PFOS induces immunosuppression in the fish larvae of marine medaka. Ecotoxicology and Environmental Safety 92, 104-111.
Farmahin, R., Williams, A., Kuo, B., Chepelev, N.L., Thomas, R.S., Barton-Maclaren, T.S., Curran, I.H., Nong, A., Wade, M.G., Yauk, C.L., 2017. Recommended approaches in the application of toxicogenomics to derive points of departure for chemical risk assessment. Archives of Toxicology 91, 2045-2065.
Fresno, C., Balzarini, M.G., Fernandez, E.A., 2014. lmdme: Linear Models on Designed Multivariate Experiments in R. Journal of Statistical Software 56, 1-16.
Giesy, J.P., Kannan, K., 2001. Global distribution of perfluorooctane sulfonate in wildlife. Environmental Science & Technology 35, 1339-1342.
Giesy, J.P., Naile, J.E., Khim, J.S., Jones, P.D., Newsted, J.L., 2010. Aquatic Toxicology of Perfluorinated Chemicals, in: Whitacre, D.M. (Ed.), Reviews of Environmental Contamination and Toxicology, Vol 202. Springer, New York, pp. 1-52.
Grandjean, P., 2018. Delayed discovery, dissemination, and decisions on intervention in environmental health: a case study on immunotoxicity of perfluorinated alkylate substances. Environmental Health 17, 62-62.
Hagenaars, A., Stinckens, E., Vergauwen, L., Bervoets, L., Knapen, D., 2014. PFOS affects posterior swim bladder chamber inflation and swimming performance of zebrafish larvae. Aquatic Toxicology 157, 225-235.
Hill, A.J., Teraoka, H., Heideman, W., Peterson, R.E., 2005. Zebrafish as a model vertebrate for investigating chemical toxicity, pp. 6-19.
Hirose, Y., Simon, J.A., Ou, H.C., 2011. Hair Cell Toxicity in Anti-cancer Drugs: Evaluating an Anti-cancer Drug Library for Independent and Synergistic Toxic Effects on Hair Cells Using the Zebrafish Lateral Line. Jaro-Journal of the Association for Research in Otolaryngology 12, 719-728.
Hoff, P.T., Van Campenhout, K., Van De Vijver, K., Covaci, A., Bervoets, L., Moens, L., Huyskens, G., Goemans, G., Belpaire, C., Blust, R., De Coen, W., 2005. Perfluorooctane sulfonic acid and organohalogen pollutants in liver of three freshwater fish species in Flanders (Belgium): relationships with biochemical and organismal effects. Environmental Pollution 137, 324-333.
Houde, M., De Silva, A.O., Muir, D.C.G., Letcher, R.J., 2011. Monitoring of Perfluorinated Compounds in Aquatic Biota: An Updated Review PFCs in Aquatic Biota. Environmental Science & Technology 45, 7962-7973.
Howe, K., Schiffer, P.H., Zielinski, J., Wiehe, T., Laird, G.K., Marioni, J.C., Soylemez, O., Kondrashov, F., Leptin, M., 2016. Structure and evolutionary history of a large family of NLR proteins in the zebrafish. Open Biology 6, 160009-160009.
Huang, H., Huang, C., Wang, L., Ye, X., Bai, C., Simonich, M.T., Tanguay, R.L., Dong, Q., 2010. Toxicity, uptake kinetics and behavior assessment in zebrafish embryos following exposure to perfluorooctanesulphonicacid (PFOS). Aquatic Toxicology 98, 139-147.
Huang, S.S.Y., Benskin, J.P., Chandramouli, B., Butler, H., Helbing, C.C., Cosgrove, J.R., 2016. Xenobiotics Produce Distinct Metabolomic Responses in Zebrafish Larvae (Danio rerio). Environmental Science & Technology 50, 6526-6535.
Jantzen, C.E., Annunziato, K.A., Bugel, S.M., Cooper, K.R., 2016. PFOS, PFNA, and PFOA sub-lethal exposure to embryonic zebrafish have different toxicity profiles in terms of morphometrics, behavior and gene expression. Aquatic Toxicology 175, 160-170.

693 Jensen, A.A., Leffers, H., Emerging endocrine disrupters: Perfluoroalkylated substances,
694 2 ed, pp. 161-169.
695 Jin, Y., Saito, N., Harada, K.H., Inoue, K., Koizumi, A., 2007. Historical trends in human
696 serum levels of perfluorooctanoate and perfluorooctane sulfonate in Shenyang, China.
697 The Tohoku journal of experimental medicine 212, 63-70.
698 Kannan, K., Tao, L., Sinclair, E., Pastva, S.D., Jude, D.J., Giesy, J.P., 2005. Perfluorinated
699 compounds in aquatic organisms at various trophic levels in a Great Lakes food chain.
700 Archives of Environmental Contamination and Toxicology 48, 559-566.
701 Kato, K., Wong, L.-Y., Basden, B.J., Calafat, A.M., 2013. Effect of temperature and
702 duration of storage on the stability of polyfluoroalkyl chemicals in human serum.
703 Chemosphere 91, 115-117.
704 Kato, K., Ye, X., Calafat, A.M., 2015. PFASs in the General Population, pp. 51-76.
705 Kimmel, C.B., Ballard, W.W., Kimmel, S.R., Ullmann, B., Schilling, T.F., 1995. Stages of
706 embryonic development of the zebrafish. Dev Dyn 203, 253-310.
707 Kluska, K., Adamczyk, J., Krężel, A., 2018. Metal binding properties, stability and
708 reactivity of zinc fingers, pp. 18-64.
709 Kunacheva, C., Tanaka, S., Fujii, S., Boontanon, S.K., Musirat, C., Wongwattana, T.,
710 Shivakoti, B.R., 2011. Mass flows of perfluorinated compounds (PFCs) in central
711 wastewater treatment plants of industrial zones in Thailand. Chemosphere 83, 737-
712 744.
713 Lai, K.P., Ng, A.H.M., Wan, H.L., Wong, A.Y.M., Leung, C.C.T., Li, R., Wong, C.K.C., 2018.
714 Dietary Exposure to the Environmental Chemical, PFOS on the Diversity of Gut
715 Microbiota, Associated With the Development of Metabolic Syndrome. Frontiers in
716 Microbiology 9, 11.
717 Laity, J.H., Lee, B.M., Wright, P.E., 2001. Zinc finger proteins: New insights into
718 structural and functional diversity. Elsevier Current Trends, pp. 39-46.
719 Lau, C., 2015. Perfluorinated compounds: an overview. Humana Press, Cham, pp. 1-21.
720 Lau, C., Anitole, K., Hodes, C., Lai, D., Pfahles-Hutchens, A., Seed, J., 2007.
721 Perfluoroalkyl acids: A review of monitoring and toxicological findings. Toxicological
722 Sciences 99, 366-394.
723 Li, B., Dewey, C.N., 2011. RSEM: accurate transcript quantification from RNA-Seq data
724 with or without a reference genome. Bmc Bioinformatics 12, 323-323.
725 Li, M.H., 2009. Toxicity of Perfluorooctane Sulfonate and Perfluorooctanoic Acid to
726 Plants and Aquatic Invertebrates. Environmental Toxicology 24, 95-101.
727 Li-Villarreal, N., Forbes, M.M., Loza, A.J., Chen, J., Ma, T., Helde, K., Moens, C.B., Shin,
728 J., Sawada, A., Hindes, A.E., Dubrulle, J., Schier, A.F., Longmore, G.D., Marlow, F.L.,
729 Solnica-Krezel, L., 2016. Dachsous1b cadherin regulates actin and microtubule
730 cytoskeleton during early zebrafish embryogenesis. Development 143, 1832-1832.
731 Loos, R., Carvalho, R., António, D.C., Comero, S., Locoro, G., Tavazzi, S., Paracchini, B.,
732 Ghiani, M., Lettieri, T., Blaha, L., Jarosova, B., Voorspoels, S., Servaes, K., Haglund, P.,
733 Fick, J., Lindberg, R.H., Schwesig, D., Gawlik, B.M., 2013. EU-wide monitoring survey on
734 emerging polar organic contaminants in wastewater treatment plant effluents. Water
735 Research 47, 6475-6487.
736 Love, M.I., Huber, W., Anders, S., 2014. Moderated estimation of fold change and
737 dispersion for RNA-seq data with DESeq2. Genome Biology 15, 550-550.

738 Luo, K., Li, Y., Xia, L., Hu, W., Gao, W., Guo, L., Tian, G., Qi, Z., Yuan, H., Xu, Q., 2017.
739 Analysis of the expression patterns of the novel large multigene TRIM gene family
740 (finTRIM) in zebrafish. Fish & Shellfish Immunology 66, 224-230.
741 Lyu, X.-J., Li, W.-W., Lam, P.K.S., Yu, H.-Q., 2015. Insights into perfluorooctane
742 sulfonate photodegradation in a catalyst-free aqueous solution. Scientific Reports 5,
743 9353-9353.
744 Martínez, R., Esteve-Codina, A., Herrero-Nogareda, L., Ortiz-Villanueva, E., Barata, C.,
745 Tauler, R., Raldúa, D., Piña, B., Navarro-Martín, L., 2018. Dose-dependent
746 transcriptomic responses of zebrafish eleutheroembryos to Bisphenol A.
747 Environmental Pollution.
748 Mashoof, S., Criscitiello, M., 2016. Fish immunoglobulins. Biology 5, 45-45.
749 Möller, A.-M., Korytář, T., Köllner, B., Schmidt-Posthaus, H., Segner, H., 2014. The
750 teleostean liver as an immunological organ: Intrahepatic immune cells (IHICs) in
751 healthy and benzo[a]pyrene challenged rainbow trout (Oncorhynchus mykiss).
752 Developmental & Comparative Immunology 46, 518-529.
753 Mortazavi, A., Williams, B.A., McCue, K., Schaeffer, L., Wold, B., 2008. Mapping and
754 quantifying mammalian transcriptomes by RNA-Seq. Nature Methods 5, 621-628.
755 Mould, A.P., McLeish, J.A., Huxley-Jones, J., Goonesinghe, A.C., Hurlstone, A.F.L., Boot-
756 Handford, R.P., Humphries, M.J., 2006. Identification of multiple integrin β1 homologs
757 in zebrafish (Danio rerio). BMC Cell Biology 7, 24-24.
758 Mushtaq, M.Y., Verpoorte, R., Kim, H.K., 2013. Zebrafish as a model for systems
759 biology. Biotechnology and Genetic Engineering Reviews, Vol 29, Issue 2 29, 187-205.
760 Ng, T.B., Li, W.W., Yeung, H.W., 1989. Effects of lectins with various carbohydrate
761 binding specificities on lipid metabolism in isolated rat and hamster adipocytes.
762 International Journal of Biochemistry 21, 149-156.
763 NPT, National Toxicology Program, 2016. NTP monograph: Immunotoxicity associated
764 with exposure to perfluorooctanoic acid or perfluorooctane sulfonate. US Department
765 of Human and Health Services.
766 OECD, 2002. Co-operation on existing chemicals: hazard assessment of
767 perfluorooctane sulfonate (PFOS) and its salts, pp. 1-362.
768 OECD, 2013. Test No. 236: Fish Embryo Acute Toxicity (FET) Test. OECD Publishing.
769 Olsen, G.W., 2015. PFAS Biomonitoring in Higher Exposed Populations. Toxicological
770 Effects of Perfluoroalkyl and Polyfluoroalkyl Substances, 77-125.
771 Ortiz-Villanueva, E., Jaumot, J., Martinez, R., Navarro-Martin, L., Pina, B., Tauler, R.,
772 2018. Assessment of endocrine disruptors effects on zebrafish (Danio rerio) embryos
773 by untargeted LC-HRMS metabolomic analysis. The Science of the total environment
774 635, 156-166.
775 Paul, A.G., Jones, K.C., Sweetman, A.J., 2009. A First Global Production, Emission, And
776 Environmental Inventory For Perfluorooctane Sulfonate. Environmental Science &
777 Technology 43, 386-392.
778 Peden-Adams, M.M., Keller, J.M., Eudaly, J.G., Berger, J., Gilkeson, G.S., Keil, D.E.,
779 2008. Suppression of humoral immunity in mice following exposure to perfluorooctane
780 sulfonate. Toxicological Sciences 104, 144-154.
781 Phillips, J.R., Svoboda, D.L., Tandon, A., Patel, S., Sedykh, A., Mav, D., Kuo, B., Yauk,
782 C.L., Yang, L., Thomas, R.S., Gift, J.S., Davis, J.A., Olysyzk, L., Merrick, B.A., Paules, R.S.,
783 Parham, F., Saddler, T., Shah, R.R., Auerbach, S.S., 2018. BMDExpress 2: Enhanced
784 transcriptomic dose-response analysis workflow. Bioinformatics (Oxford, England).

785 Quesada-Garcia, A., Encinas, P., Valdehita, A., Baumann, L., Segner, H., Coll, J.M.,
786 Navas, J.M., 2016. Thyroid active agents T3 and PTU differentially affect immune gene
787 transcripts in the head kidney of rainbow trout (Oncorynchus mykiss). Aquatic
788 Toxicology 174, 159-168.
789 R_Development_Core_Team, 2008. R: A language and environment for statistical
790 computing. R Foundation for Statistical Computing, Vienna, Austria.
791 Raldua, D., Otero, D., Fabra, M., Cerda, J., 2008. Differential localization and regulation
792 of two aquaporin-1 homologs in the intestinal epithelia of the marine teleost Sparus
793 aurata. American Journal of Physiology-Regulatory Integrative and Comparative
794 Physiology 294, R993-R1003.
795 Raldúa, D., Piña, B., 2014. In vivo zebrafish assays for analyzing drug toxicity. Expert
796 Opinion on Drug Metabolism and Toxicology 10, 685-697.
797 Rehberger, K., Werner, I., Hitzfeld, B., Segner, H., Baumann, L., 2017. 20 Years of fish
798 immunotoxicology – what we know and where we are. Critical Reviews in Toxicology
799 47, 516-542.
800 Reuter, J.A., Spacek, D.V., Snyder, M.P., 2015. High-Throughput Sequencing
801 Technologies.
802 Roca, F.J., Mulero, I., López-Muñoz, A., Sepulcre, M.P., Renshaw, S.A., Meseguer, J.,
803 Mulero, V., 2008. Evolution of the inflammatory response in vertebrates: fish TNF-
804 alpha is a powerful activator of endothelial cells but hardly activates phagocytes.
805 Journal of immunology (Baltimore, Md. : 1950) 181, 5071-5081.
806 Rodriguez-Jorquera, I.A., Colli-Dula, R.C., Kroll, K., Jayasinghe, B.S., Marco, M.V.P.,
807 Silva-Sanchez, C., Toor, G.S., Denslow, N.D., 2019. Blood Transcriptomics Analysis of
808 Fish Exposed to Perfluoro Alkyls Substances: Assessment of a Non-Lethal Sampling
809 Technique for Advancing Aquatic Toxicology Research. Environmental Science &
810 Technology 53, 1441-1452.
811 Rodriguez-Jorquera, I.A., Kroll, K.J., Toor, G.S., Denslow, N.D., 2015. Transcriptional and
812 physiological response of fathead minnows (Pimephales promelas) exposed to urban
813 waters entering into wildlife protected areas. Environmental Pollution 199, 155-165.
814 Rodriguez-Jorquera, I.A., Silva-Sanchez, C., Strynar, M., Denslow, N.D., Toor, G.S., 2016.
815 Footprints of Urban Micro-Pollution in Protected Areas: Investigating the Longitudinal
816 Distribution of Perfluoroalkyl Acids in Wildlife Preserves. PLoS One 11.
817 Sato, I., Kawamoto, K., Nishikawa, Y., Tsuda, S., Yoshida, M., Yaegashi, K., Saito, N., Liu,
818 W., Jin, Y., 2009. Neurotoxicity of perfluorooctane sulfonate (PFOS) in rats and mice
819 after single oral exposure. The Journal of toxicological sciences 34, 569-574.
820 Scholz, S., Mayer, I., 2008. Molecular biomarkers of endocrine disruption in small
821 model fish. Mol Cell Endocrinol 293, 57-70.
822 Segner, H., Verburg-van Kemenade, B.M.L., Chadzinska, M., 2017. The
823 immunomodulatory role of the hypothalamus-pituitary-gonad axis: Proximate
824 mechanism for reproduction-immune trade offs? Developmental & Comparative
825 Immunology 66, 43-60.
826 Shi, X., Yeung, L.W.Y., Lam, P.K.S., Wu, R.S.S., Zhou, B., 2009. Protein Profiles in
827 Zebrafish (Danio rerio) Embryos Exposed to Perfluorooctane Sulfonate. Toxicological
828 Sciences 110, 334-340.
829 Shi, X.J., Du, Y.B., Lam, P.K.S., Wu, R.S.S., Zhou, B.S., 2008. Developmental toxicity and
830 alteration of gene expression in zebrafish embryos exposed to PFOS. Toxicology and
831 Applied Pharmacology 230, 23-32.

Spulber, S., Kilian, P., Ibrahim, W.N.W., Onishchenko, N., Ulhaq, M., Norrgren, L., Negri, S., Di Tuccio, M., Ceccatelli, S., 2014. PFOS induces behavioral alterations, including spontaneous hyperactivity that is corrected by dexamfetamine in zebrafish larvae. PLoS One 9, e94227-e94227.
Stegeman, J.J., Goldstone, J.V., Hahn, E., 2010. Perspectives on zebrafish as a model in environmental toxicology, in: StF. Perry, M.E., AP Farrell, Colin, J.B. (Eds.), Fish Physiology. Academic Press, pp. 367-439.
Stengel, D., Zindler, F., Braunbeck, T., 2017. An optimized method to assess ototoxic effects in the lateral line of zebrafish (Danio rerio) embryos. Comparative Biochemistry and Physiology Part C: Toxicology & Pharmacology 193, 18-29.
Strahle, U., Scholz, S., Geisler, R., Greiner, P., Hollert, H., Rastegar, S., Schumacher, A., Selderslaghs, I., Weiss, C., Witters, H., Braunbeck, T., 2012. Zebrafish embryos as an alternative to animal experiments--a commentary on the definition of the onset of protected life stages in animal welfare regulations. Reprod Toxicol 33, 128-132.
Stylianou, M., Bjornsdotter, M.K., Olsson, P.E., Jogsten, I.E., Jass, J., 2019. Distinct transcriptional response of Caenorhabditis elegans to different exposure routes of perfluorooctane sulfonic acid. Environmental Research 168, 406-413.
Sun, G., Liu, K., Wang, X., Liu, X., He, Q., Hsiao, C.D., 2015. Identification and expression analysis of zebrafish (Danio rerio) E-selectin during embryonic development. Molecules 20, 18539-18550.
Suo, C., Fan, Z., Zhou, L., Qiu, J., 2017. Perfluorooctane sulfonate affects intestinal immunity against bacterial infection. Scientific Reports 7, 5166-5166.
Thienpont, B., Tingaud-Sequeira, A., Prats, E., Barata, C., Babin, P.J., Raldua, D., 2011. Zebrafish Eleutheroembryos Provide a Suitable Vertebrate Model for Screening Chemicals that Impair Thyroid Hormone Synthesis. Environmental Science & Technology 45, 7525-7532.
van der Aa, L.M., Jouneau, L., Laplantine, E., Bouchez, O., Van Kemenade, L., Boudinot, P., 2012. FinTRIMs, fish virus-inducible proteins with E3 ubiquitin ligase activity. Developmental & Comparative Immunology 36, 433-441.
Vasta, G.R., Nita-Lazar, M., Giomarelli, B., Ahmed, H., Du, S., Cammarata, M., Parrinello, N., Bianchet, M.A., Amzel, L.M., 2011. Structural and functional diversity of the lectin repertoire in teleost fish: Relevance to innate and adaptive immunity. Developmental and Comparative Immunology 35, 1388-1399.
Vedagiri, U.K., Anderson, R.H., Loso, H.M., Schwach, C.M., 2018. Ambient levels of PFOS and PFOA in multiple environmental media. Remediation 28, 9-51.
Versteeg, G.A., Rajsbaum, R., Sanchez-Aparicio, M.T., Maestre, A.M., Valdiviezo, J., Shi, M., Inn, K.S., Fernandez-Sesma, A., Jung, J., Garcia-Sastre, A., 2013. The E3-Ligase TRIM Family of Proteins Regulates Signaling Pathways Triggered by Innate Immune Pattern-Recognition Receptors. Immunity 38, 384-398.
Webster, A.F., Chepelev, N., Gagne, R., Kuo, B., Recio, L., Williams, A., Yauk, C.L., 2015. Impact of Genomics Platform and Statistical Filtering on Transcriptional Benchmark Doses (BMD) and Multiple Approaches for Selection of Chemical Point of Departure (PoD). PLoS One 10.
White, S.S., Fenton, S.E., Hines, E.P., 2011. Endocrine disrupting properties of perfluorooctanoic acid. J Steroid Biochem Mol Biol 127, 16-26.
Woo, J.S., Imm, J.H., Min, C.K., Kim, K.J., Cha, S.S., Oh, B.H., 2006. Structural and functional insights into the B30.2/SPRY domain. Embo Journal 25, 1353-1363.

879 Yang, L., Allen, B.C., Thomas, R.S., 2007. BMDExpress: a software tool for the
880 benchmark dose analyses of genomic data. Bmc Genomics 8.
881 Zeng, X.W., Qian, Z., Vaughn, M., Xian, H., Elder, K., Rodemich, E., Bao, J., Jin, Y.H.,
882 Dong, G.H., 2015. Human serum levels of perfluorooctane sulfonate (PFOS) and
883 perfluorooctanoate (PFOA) in Uyghurs from Sinkiang-Uighur Autonomous Region,
884 China: background levels study. Environmental Science and Pollution Research 22,
885 4736-4746.
886 Zeng, Z.T., Song, B., Xiao, R., Zeng, G.M., Gong, J.L., Chen, M., Xu, P.A., Zhang, P., Shen,
887 M.C., Yi, H., 2019. Assessing the human health risks of perfluorooctane sulfonate by in
888 vivo and in vitro studies. Environment International 126, 598-610.
889 Zhang, X., Zhao, H., Chen, Y., Luo, H., Yang, P., Yao, B., 2015. A zebrafish (Danio rerio)
890 bloodthirsty member 20 with E3 ubiquitin ligase activity involved in immune response
891 against bacterial infection. Biochemical and Biophysical Research Communications 457,
892 83-89.
893 Zhang, Y.H., Wang, J., Dong, G.H., Liu, M.M., Wang, D., Zheng, L., Jin, Y.H., 2013.
894 Mechanism of perfluorooctanesulfonate (PFOS)-induced apoptosis in the immunocyte.
895 Journal of Immunotoxicology 10, 49-58.

896

Figure Legends

Figure 1. Morphometric measurements of zebrafish embryos treated with different concentrations of PFOS from 2 to 5 dpf. **A)** Representative pictures of eleutheroembryos at 5 dpf exposed to different concentrations of PFOS. **B)** Description of morphological traits measured from lateral (I) and dorsoventral (II) images. Measured traits were the following: body length (BL), head-trunk angle (HTA), yolk sac area (YSA), swim bladder area (SBA), eye length (EL), eye width (EW), head width (HW), inter-ocular distance (IOD) and eye-snout distance (ESD). Scale bar: 1.0 mm. **C)** Quantitative analyses of the effects of PFOS on the morphological parameters shown in Figure 1C (n=50 larvae/group). All measures are expressed in mm except YSA and SBA (expressed in mm^2), and HTA (expressed in arc degrees). Different low-case letters in each graph indicate statistically differences between experimental groups (Kruskal-Wallis tests plus Dunn's pairwise multiple comparisons with Bonferroni correction $p < 0.05$). Means and SEM (standard error of the mean) are represented. Morphological parameters were not determined at the highest concentrations in the exposure (10 and 100 mg/L) due to their high rates of mortality (82 and 100 %, respectively). **D)** Immunofluorescent analyses of olfactory epithelium (A', B') and neuromasts (C', D') structures in 5 dpf eleutheroembryos after exposure to 1 mg/L PFOS. A'-B': Dorsal view of the head of a representative control (A') and 1 mg/L PFOS-exposed (B') eleutheroembryo immunolabeled with a double whole-mount immunofluorescence using anti-parvalbumin (*Parv*) and anti-acetylated alpha tubulin (*α-AT*) primary antibodies. The former antibody labels ciliated and microvillous neurons in the sensory olfactory epithelium, whereas the later labels kinocilia of ciliated nonsensory cells and the cilia of the ciliated sensory neurons. The region encircled by a dashed line correspond with the olfactory pits. C'-D': Lateral view (head on the left side) of a representative control (C') and PFOS-exposed (D') eleutheroembryo immunolabeled with anti-acetylated alpha tubulin primary antibody, labeling the neuromasts (nm). Scale bars: 100 µm.

Figure 2. Effects of PFOS on zebrafish embryo transcriptome. **A)** Heatmap showing concentration changes corresponding to the 1434 transcripts identified by ANOVA-PLS as differentially expressed genes (DEGs) in at least one of the experimental groups.

Values were centered to the average of control samples and log2 transformed. Color scale ranges from blue (strongly underexpressed relative to control) to red (strongly overexpressed); white cells correspond to control values (fold change = 0). Both rows (genes) and columns (samples) were grouped by hierarchical clustering; the corresponding dendrograms are shown at the left and the top of the panel, respectively. **B)** Results from medoid PAM clustering of DEGs by PCA analysis showing the two defined clusters labeled in blue and red (clusters A and B, respectively). The two first components (PC1 and PC2) of the PCA explained 49.07% of total variability. **C)** Heatmaps of the genes classified in cluster A (left) and B (right) by the medoid PAM clustering of DEGs; legend as in Figure 2A. **D)** Normalized abundance values for all the genes included in each of the two clusters (cluster A at left, which contains the underexpressed genes due to PFOS exposure, and cluster B at right, where the genes that enhance their abundance among the exposure are placed). Low-case letters at the top of each graph indicate statistical differences (parametric ANOVA + Tukey's B post-hoc test with all pairwise comparisons, $p \leq 0.05$). Boxes include values between the 1st and 3rd quartiles, thick bars indicate average values and whiskers cover the total distribution, except for outliers (circles).

Figure 3. Functional analyses of the genes categorized as DEGs, distributed in clusters as previously shown in Figure 2. **A)** Distribution of DEGs among the two defined clusters (columns) and the different functional modules (rows). Only clusters with at least four hits in at least one of the clusters are shown. For simplicity, the "Signal" keyword module included in Table 1 was not considered in the figure. Numbers indicate the number of DEGs for each functional module classified in cluster A (left) or B (right). Cell colors represent the relative importance of transcripts associated to each pathway for each cluster (as a heat code: from red -less importance- to white -more importance-). Two cells with the same color correspond to identical fraction of DEGs (i.e. the same importance). Complete David Functional Analysis can be found at Table 1. **B)** Network representation of DEGs, which are represented by dots and colored as before (cluster A in blue and cluster B in red). Networking was carry out according to the adscription of the DEGs to functional modules (GO:biological process and KEGG databases were used, codes for each module are given as nodes). Color ellipses

encircle groups of functional modules with particular interest and relevance (see section 3.4.).

Table 1

Click here to download Table: PFOS_Table T1_R1.xlsx

Table 1. David Functional Analysis[a)] results for both gene clusters, individual and combined (only results with FDR≤5%)

Category	Term	# of DEGs	Fold Enrichment	*p* value	FDR
Cluster 1 (underrepresented in treated samples relative to controls)					
INTERPRO	IPR001870:B30.2/SPRY domain	24	3.5	4.32E-07	6.66E-04
INTERPRO	IPR006574:SPRY-associated	20	3.4	9.36E-06	0.014
KEGG_PATHWAY	dre04630:Jak-STAT signaling pathway	12	5.2	1.59E-05	0.017
INTERPRO	IPR003877:SPla/RYanodine receptor SPRY	20	3.2	1.48E-05	0.023
INTERPRO	IPR001507:Zona pellucida domain	9	6.4	7.75E-05	0.120
GOTERM_BP_DIRECT	GO:0016567~protein ubiquitination	16	3.4	9.09E-05	0.133
INTERPRO	IPR003879:Butyrophylin-like	18	3.0	1.10E-04	0.169
GOTERM_BP_DIRECT	GO:0019885~antigen processing and presentation of endogenous peptide antigen via MHC class I	4	25.7	3.52E-04	0.515
INTERPRO	IPR013320:Concanavalin A-like lectin/glucanase	25	2.2	4.27E-04	0.656
GOTERM_MF_DIRECT	GO:0008270~zinc ion binding	47	1.6	0.002	2.160
KEGG_PATHWAY	dre04060:Cytokine-cytokine receptor interaction	11	3.2	0.002	2.341
INTERPRO	IPR011029:Death-like domain	9	3.7	0.003	4.393
GOTERM_BP_DIRECT	GO:0007160~cell-matrix adhesion	6	5.9	0.003	4.807
Cluster 2 (overrepresented in treated samples relative to controls)					
GOTERM_MF_DIRECT	GO:0008374~O-acyltransferase activity	5	11.5	7.98E-04	1.149
UP_KEYWORDS	Lipid transport	6	7.6	0.001	1.335
GOTERM_BP_DIRECT	GO:0006869~lipid transport	8	5.1	9.50E-04	1.408
KEGG_PATHWAY	dre00564:Glycerophospholipid metabolism	9	4.0	0.002	1.748
Clusters 1 + 2					
KEGG_PATHWAY	dre04060:Cytokine-cytokine receptor interaction	19	2.6	2.48E-04	0.285
KEGG_PATHWAY	dre04630:Jak-STAT signaling pathway	15	3.1	2.67E-04	0.307
GOTERM_MF_DIRECT	GO:0008374~O-acyltransferase activity	7	7.6	2.13E-04	0.324
UP_KEYWORDS	Signal	218	1.2	9.33E-04	1.178
GOTERM_CC_DIRECT	GO:0005615~extracellular space	40	1.7	0.001	1.531
GOTERM_MF_DIRECT	GO:0004888~transmembrane signaling receptor activity	24	2.1	0.001	2.160
GOTERM_BP_DIRECT	GO:0051607~defense response to virus	8	4.6	0.002	2.354
INTERPRO	IPR011029:Death-like domain	13	2.9	0.002	2.611

[a)] https://david.ncifcrf.gov

Figure 1

Click here to download high resolution image

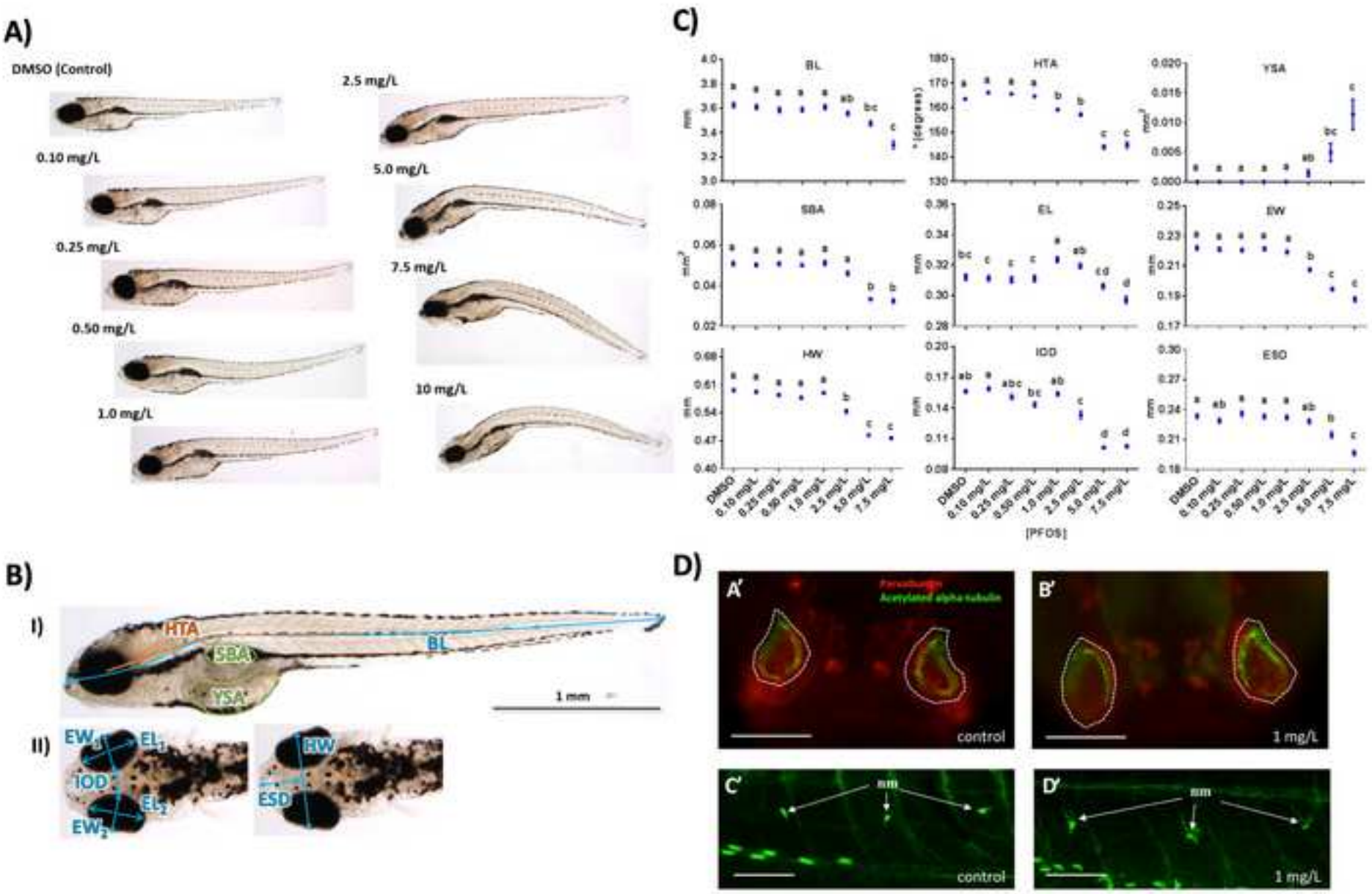

Figure 1

Figure 2
Click here to download high resolution image

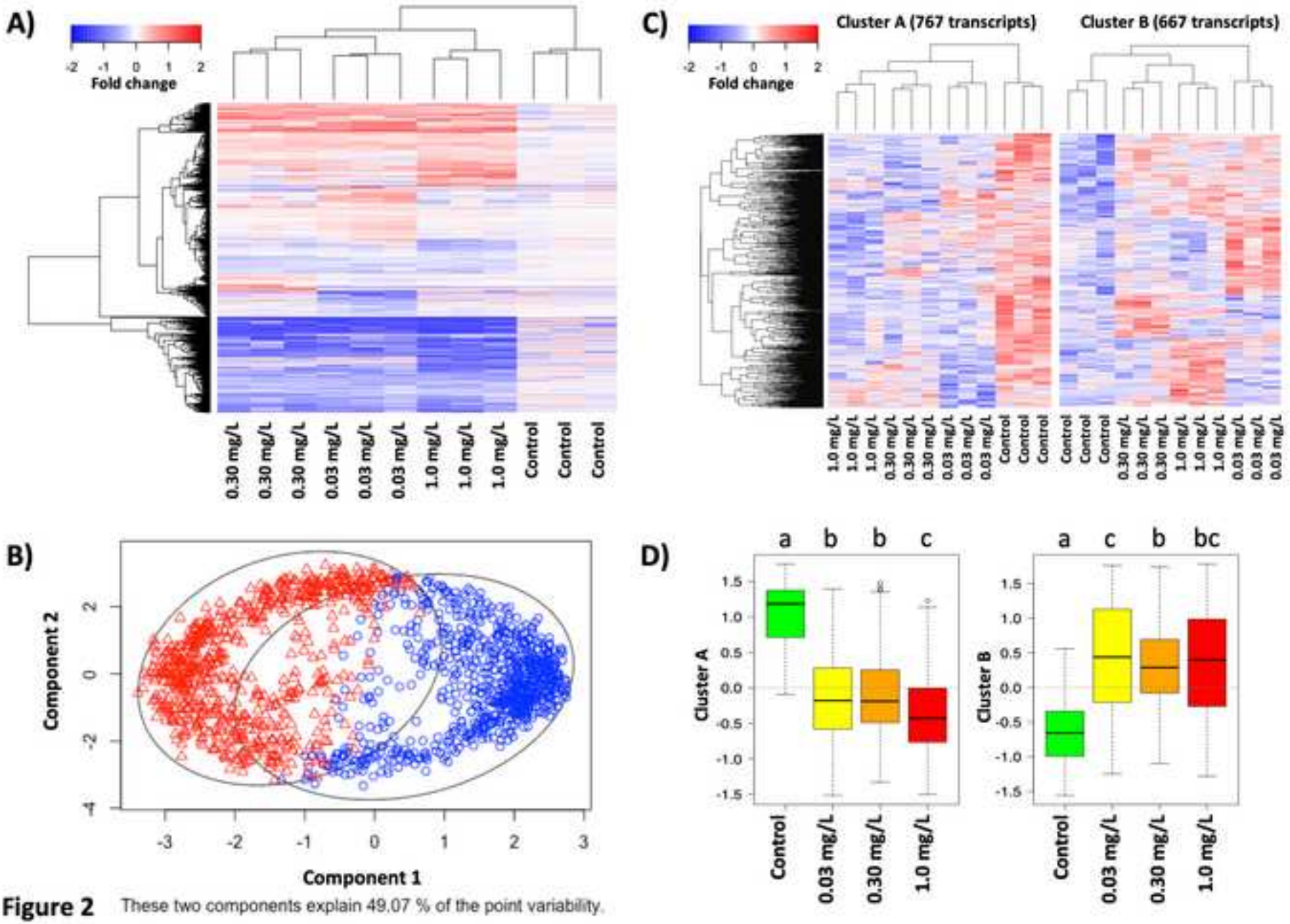

Figure 2 These two components explain 49.07 % of the point variability.

Figure 3

Click here to download high resolution image

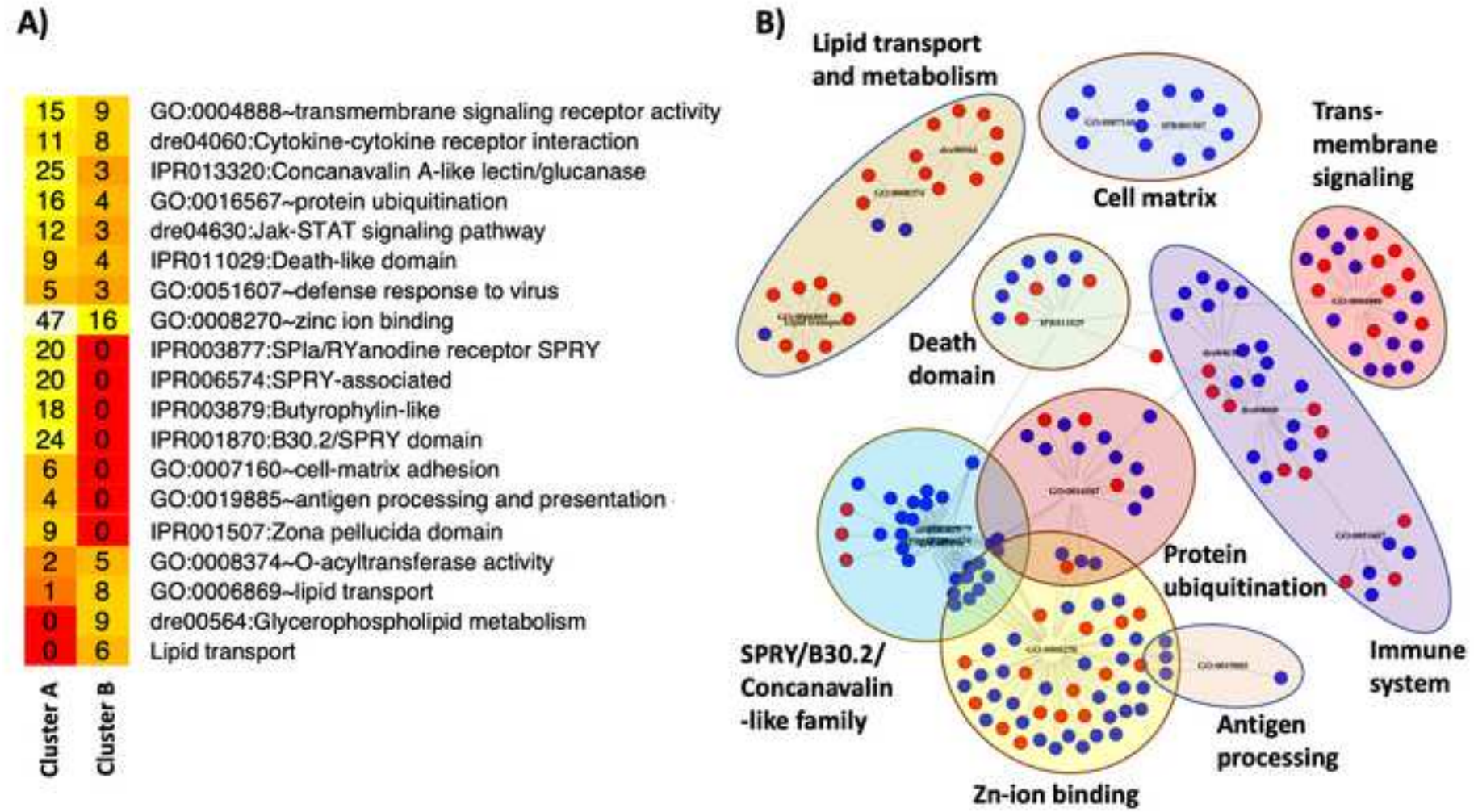

Figure 3

Supplementary material

Unravelling the mechanisms of PFOS toxicity by combining morphological and transcriptomic analyses in zebrafish embryos

Rubén Martínez[1,2], Laia Navarro-Martín[1], Chiara Luccarelli[1], Anna E. Codina[3,4], Demetrio Raldúa[1], Carlos Barata[1], Romà Tauler[1], Benjamin Piña[1]*

[1]IDAEA-CSIC. Jordi Girona, 18. 08034 Barcelona, Spain

[2]Universitat de Barcelona (UB), Barcelona, 08007, Spain

[3]CNAG-CRG, Centre for Genomic Regulation (CRG), Barcelona Institute of Science and Technology (BIST), Barcelona, 08028, Spain

[4]Universitat Pompeu Fabra (UPF), Barcelona, 08003, Spain

* Corresponding author: Benjamin Piña, Institute of Environmental Assessment and Water Research, IDAEA-CSIC, Jordi Girona 18, 08034 Barcelona, Spain TEL. +34 93 4006100, ext 1551; E-mail: bpcbmc@cid.csic.es

Supplementary methods

Supp. method 1: RT-qPCR analysis

Total RNA from 9 replicates (10 larvae per replicate) was extracted using the Trizol method following the manufacturer protocol (Ambion, Thermo Fisher Scientific). Extracted concentrations were assessed with a NanoDrop® 8000 UV-Vis Spectrophotometer (Thermo Scientific) and genomic undesirable DNA was removed with Ambion™ DNase I (Thermo Fisher Scientific). RNA was reverse-transcribed to cDNA using Transcriptor First Strand cDNa Sythesis Kit (Roche Diagnostics) following manufacturer's protocols. A no-RT negative controls were also prepared by replacing the RT enzyme with water. To measure the relative mRNA abundances of target genes, quantitative real-time polymerase chain reactions (qRT-PCR) were carry out, using a LightCycler® 480 Real-Time PCR System (Roche Diagnostics, Mannheim, Germany). The amplification program consisted of 10 min at 95 °C, followed by 45 cycles (10 s at 95 °C, 30 s at 60 °C). After the amplification, a dissociation analysis was also programmed (obtaining a melting curve) to evaluate the specificity of the reaction. The amplification reaction efficiency for each gene was assessed (**Supplementary Table ST3**). Relative transcript abundance were calculated from maximum of the second derivative (Cp, calculated by technical duplicates) of their respective amplification curves. PPIAa was used as a reference gene. Cp values for target genes (Cp_{tg}) were normalized to the average Cp values of reference gene, following the equation: $\Delta Cp_{tg} = Cp_{PPIAa} - Cp_{tg}$. Transcript abundance changes in samples were calculated by the ΔΔCp method [1]: $\Delta\Delta Cp_{tg} = \Delta Cp_{tg}$ (control group) − ΔCp_{tg} (exposed group). From those ΔΔCptg values, fold-change ratios were obtained.

[1] M. W. Pfaffl, “A new mathematical model for relative quantification in real-time RT-PCR,” *Nucleic Acids Res.*, 2001.

Supplementary Table ST1. RNA-Seq readings and mapping quality statistics.

Sample Barcode	Sample Name	Number of FLIs	Million read-pairs (or reads)	Yield (Gb)	Trimmed yield (Gb)	Avg PhiX error r1	Avg PhiX error r2	Organism	Reference	Avg % unique	Avg % unmapped	Avg % duplicate	Avg % difference r1	Avg % difference r2	Avg alignment insert size
AB3131	PFOS (2-5) Ctl R1	2	32.569	4.950	4.949	0.25	0.36	*Danio rerio*	drerio.GRCz10	80.60	2.06	18.38	1.31	1.33	144.00
AB3132	PFOS (2-5) 0,03ppm R1	1	41.359	6.287	6.286	0.17	0.31	*Danio rerio*	drerio.GRCz10	81.07	1.16	31.63	1.17	1.16	137.00
AB3133	PFOS (2-5) 0,3ppm R1	2	36.463	5.542	5.541	0.16	0.33	*Danio rerio*	drerio.GRCz10	79.42	1.82	21.92	1.26	1.26	141.00
AB3134	PFOS (2-5) 1ppm R1	2	42.264	6.424	6.422	0.17	0.34	*Danio rerio*	drerio.GRCz10	82.04	1.45	21.12	1.15	1.17	153.00
AB3139	PFOS (2-5) Ctl R3	2	39.487	6.002	6.000	0.17	0.34	*Danio rerio*	drerio.GRCz10	81.91	1.64	22.30	1.17	1.18	142.00
AB3140	PFOS (2-5) 0,03ppm R3	2	35.693	5.426	5.424	0.17	0.34	*Danio rerio*	drerio.GRCz10	83.27	1.52	22.27	1.18	1.20	148.00
AB3141	PFOS (2-5) 0,3ppm R3	1	37.656	5.724	5.717	0.14	0.28	*Danio rerio*	drerio.GRCz10	82.20	1.44	30.26	1.17	1.29	138.00
AB3142	PFOS (2-5) 1ppm R3	1	48.043	7.303	7.302	0.17	0.31	*Danio rerio*	drerio.GRCz10	83.20	1.16	30.91	1.24	1.23	137.00
AB3143	PFOS (2-5) Ctl R2	1	36.218	5.505	5.501	NA	NA	*Danio rerio*	drerio.GRCz10	82.41	1.53	31.48	1.13	1.15	151.00
AB3144	PFOS (2-5) 0,03ppm R2	1	38.790	5.896	5.892	NA	NA	*Danio rerio*	drerio.GRCz10	81.79	1.25	30.09	1.13	1.15	148.00
AB3145	PFOS (2-5) 0,3ppm R2	1	40.419	6.144	6.139	NA	NA	*Danio rerio*	drerio.GRCz10	85.39	1.33	32.59	1.16	1.20	153.00
AB3146	PFOS (2-5) 1ppm R2	2	36.776	5.590	5.589	0.16	0.33	*Danio rerio*	drerio.GRCz10	86.33	1.69	27.59	1.21	1.26	148.50

Column description	
Sample Barcode	Unique internal CNAG identifier of the sample
Sample Name	Sample name provided by the collaborator
Number of FLIs	Number of sequencing Flowcell Lane Index units for this sample (equivalent to the number of times the sample has been sequenced)
Million read-pairs (or reads)	Total million read-pairs (or reads for single-end runs) that passed Illumina filter
Yield (Gb)	Total yield in Gigabases from the read-pairs (or reads for single-end runs) that passed Illumina filter
Trimmed yield (Gb)	Trimmed yield in Gigabases from the read-pairs (or reads for single-end runs) that passed Illumina filter
Avg PhiX error r1	Average % mismatches between the spiked-in PhiX read 1 and the PhiX reference
Avg PhiX error r2	Average % mismatches between the spiked-in PhiX read 2 and the PhiX reference
Organism	Sample's organism according to submitter
Reference	Reference sequence (genome, transcriptome, contigs...) to which the reads have been mapped
Avg % unique	Average % of reads aligning to a single location in the reference
Avg % unmapped	Average % of reads not aligning to any location in the reference
Avg % duplicate	Average % of read-pairs (or reads, for single-end runs) that map exactly at the same location in the reference as another read-pair
Avg % difference r1	Average % mismatches between read 1 and the reference
Avg % difference r2	Average % mismatches between read 2 and the reference
Avg alignment insert size	Average mapping distance between read 1 and read 2

Supplementary Table ST2. Categorical morphological measurements in 5 dpf eleutheroembryos.

	Scoliosis		Tail mal-formation (dorsoventral and lateral)	
Group (mg/L of PFOS)	n/total	Statistical significance[a)]	n/total	Statistical significance
Control	0/50	n/a	4/100	n/a
0.10	0/50	n/a	4/100	n/a
0.25	0/49	n/a	5/98	n/a
0.50	0/50	n/a	6/100	n/a
1.0	0/50	n/a	11/100	n/a
2.5	1/50	n/a	17/100	**
5.0	1/50	**	42/100	***
7.5	18/48	***	45/96	***

a)Fisher exact probability test: $p < 0.05$ (*), $p < 0.01$ (**), $p < 0.001$ (***).

Supplementary Table ST3. Efficiency and accession numbers of qPCR primers used in this study

Gene Name	Accesion nº	Description	Forward-primer	Reverse primer	Efficiency	R^2
ppiaa	NM_212758.1	peptidylprolyl isomerase Aa (cyclophilin A)	GGGTGGTAATGGAGCTGAGA	AATGGACTTGCCACCAGTTC	92.8%	>0.999
apoa4b.3	XM_001338001.6	apolipoprotein A-IV b, tandem duplicate 3	ACCAAATTAACTCTTCACAAACTTCG	ATGGCATGATAGGATGAATCGAT	92.3%	0.997
btr31	XM_005170606.2	bloodthirsty-related gene family, member 31	CATCATGCCTGCTCCTCACA	GCCGTGTCATGATCCAGAGTC	102.3%	0.982
ccl20b	NM_001113595.1	chemokine (C-C motif) ligand 20b	TGCAATCATTTTCCACACCG	CATAAGACCCGTTCTTGCGTC	98.5%	0.994
erap1a	XM_009305074.3	endoplasmic reticulum aminopeptidase 1a	CTCCGGGCTCCGCAGTAT	AGCAGTGGGACGTTCCTGTC	95.0%	0.996
erap2	NM_001123052.1	endoplasmic reticulum aminopeptidase 2	TCAGACCGGAGATTGCGTG	CCGTTCAGCCTTTTCCAAAC	103.7%	0.994
sps3b	XM_021470242.1	splA/ryanodine receptor domain and SOCS box containing 3b	ATATGATGGTTGGCATCGGG	CATCTGTGCCCAGCAGACTG	100.2%	0.993
stat1b	NM_200091.2	signal transducer and activator of transcription 1b	AGTGAAAGCTGTCGAGACGGA	CACCGAATGGATCTTGGGTT	103.2%	0.991

Table ST4. David Functional Analysis[a)] results for both gene clusters, individual and combined (only results with FDR≤5%)

Category	Term	Genes	Count	Fold Enrichment	PValue	FDR
Cluster 1 (down-regulation)						
INTERPRO	IPR001870:B30.2/SPRY domain	SI:CH211-133H13.1, SPSB1, SI:DKEY-84H14.2, BTR26, BTR29, SI:CH211-247L8.8, SI:DKEY-3H2.3, SI:CH211-120G10.1, ZGC:174180, SI:CH211-76M11.8, TRIM109, SI:DKEY-222H21.8, BTR20, SI:CH211-255G12.8, RSPRY1, ZGC:194906, FTR37, SI:DKEY-61P9.9, FTR53, FTR35, FTR56, SPSB3B, FTR30, BTR31	24	3.5	4.32E-07	6.66E-04
INTERPRO	IPR006574:SPRY-associated	SI:CH211-133H13.1, SI:DKEY-84H14.2, BTR26, BTR29, SI:CH211-247L8.8, SI:DKEY-3H2.3, SI:CH211-120G10.1, ZGC:174180, SI:CH211-76M11.8, SI:DKEY-222H21.8, BTR20, SI:CH211-255G12.8, ZGC:194906, FTR37, SI:DKEY-61P9.9, FTR53, FTR35, FTR56, FTR30, BTR31	20	3.4	9.36E-06	0.014
KEGG_PATHWAY	dre04630:Jak-STAT signaling pathway	IRF9, SI:RP71-17I16.5, IFNPHI1, STAT1B, IL6ST, IL10RB, IL20RA, LEPA, IL19L, PIK3CD, SOCS3B, IL22RA2	12	5.2	1.59E-05	0.017
INTERPRO	IPR003877:SPla/RYanodine receptor SPRY	SI:CH211-133H13.1, SPSB1, SI:DKEY-84H14.2, BTR26, BTR29, SI:CH211-247L8.8, SI:DKEY-3H2.3, SI:CH211-120G10.1, ZGC:174180, SI:CH211-76M11.8, SI:DKEY-222H21.8, BTR20, SI:CH211-255G12.8, RSPRY1, ZGC:194906, SI:DKEY-61P9.9, FTR53, FTR56, BTR31, SPSB3B	20	3.2	1.48E-05	0.023
INTERPRO	IPR001507:Zona pellucida domain	ZP3C, SI:CH211-39F2.3, ZGC:66449, SI:CH73-181M17.1, SI:DKEY-239B22.1, SI:CH211-226H7.8, ZGC:153932, SI:CH211-226H7.5, SI:CH211-226H7.6	9	6.4	7.75E-05	0.120
GOTERM_BP_DIRECT	GO:0016567~protein ubiquitination	MKRN1, TRAF1, BTR26, CCNF, HACE1, UBOX5, ASB12A, ASB18, BTR20, UVSSA, KLHL26, CAND2, KLHL38B, FBXO32, SOCS3B, BTR31	16	3.4	9.09E-05	0.133
INTERPRO	IPR003879:Butyrophylin-like	SI:CH211-133H13.1, SI:DKEY-84H14.2, BTR26, BTR29, SI:CH211-247L8.8, SI:DKEY-3H2.3, SI:CH211-120G10.1, ZGC:174180, SI:CH211-76M11.8, TRIM109, SI:DKEY-222H21.8, BTR20, SI:CH211-255G12.8, ZGC:194906, SI:DKEY-61P9.9, FTR53, BTR31, FTR56	18	3.0	1.10E-04	0.169
GOTERM_BP_DIRECT	GO:0019885~antigen processing and presentation of endogenous peptide antigen via MHC class I	ERAP1A, ERAP1B, ERAP2, TAPBPL	4	25.7	3.52E-04	0.515
INTERPRO	IPR013320:Concanavalin A-like lectin/glucanase, subgroup	SI:CH211-133H13.1, SPSB1, SI:DKEY-84H14.2, BTR26, BTR29, SI:CH211-247L8.8, SI:DKEY-3H2.3, SI:CH211-120G10.1, ZGC:174180, SI:CH211-76M11.8, TRIM109, SI:DKEY-222H21.8, BTR20, SI:CH211-255G12.8, RSPRY1, ZGC:194906, FTR37, SI:DKEY-61P9.9, FTR53, FTR35, PROS1, FTR56, SPSB3B, FTR30, BTR31	25	2.2	4.27E-04	0.656
GOTERM_MF_DIRECT	GO:0008270~zinc ion binding	MKRN1, TRAF1, ZNFX1, ZRANB1B, ZMAT2, RORC, ISL1L, ADA, FANCL, BTR20, ZFAND5B, RSPRY1, CECR1A, SETMAR, SI:CH211-244B2.2, CCS, ERAP2, XAF1, ZGC:77880, TRIM63A, FTR79, NPLOC4, THRAA, ERAP1A, ERAP1B, BTR26, BTR29, SI:CH211-247L8.8, POLE, ESR1, SIRT5, PHF11, CXXC1A, UBOX5, RNF11A, CA4B, CSRP1B, TRIM109, BHMT, FTR37, RNF25, FTR35, FTR53, RNF26, BTR31, FTR30, FTR56	47	1.6	0.002	2.160
KEGG_PATHWAY	dre04060:Cytokine-cytokine receptor interaction	TNFB, IFNPHI1, CCL20B, CCL20A.3, IL6ST, IL10RB, IL20RA, LEPA, CCR6A, TNFRSF18, IL22RA2	11	3.2	0.002	2.341
INTERPRO	IPR011029:Death-like domain	IRAK3, SI:CH211-114L13.9, CARD9, CASP9, SI:DKEY-103E21.5, SI:DKEY-61P9.9, SI:DKEY-29H14.10, SI:CH211-171L17.4, ADGRG1	9	3.7	0.003	4.393
GOTERM_BP_DIRECT	GO:0007160~cell-matrix adhesion	SI:CH211-39F2.3, HPSE, SI:CH73-181M17.1, SI:DKEY-239B22.1, SI:CH73-329N5.6, EPDL1	6	5.9	0.003	4.807
Cluster 2 (up-regulation)						
GOTERM_MF_DIRECT	GO:0008374~O-acyltransferase activity	SOAT2, LCAT, GPAT2, YKT6, GPAM	5	11.5	7.98E-04	1.149
UP_KEYWORDS	Lipid transport	APOA4B.3, OSBPL2B, APOA4B.2, APOA4B.1, OSBPL10, OSBPL11	6	7.6	0.001	1.335
GOTERM_BP_DIRECT	GO:0006869~lipid transport	APOA4B.3, OSBPL2B, APOA4B.2, APOA4B.1, OSBPL10, APOBB.1, OSBPL11, VTG6	8	5.1	9.50E-04	1.408
KEGG_PATHWAY	dre00564:Glycerophospholipid metabolism	GPD2, PMT, PLA2G12A, LCAT, PTDSS1B, PLA2G12B, GPAT2, GPAT3, GPAM	9	4.0	0.002	1.748

Table ST4 (continued). David Functional Analysis[a)] results for both gene clusters, individual and combined (only results with FDR≤5%)

Clusters 1 + 2						
KEGG_PATHWAY	dre04060:Cytokine-cytokine receptor interaction	CCL20B, IL6ST, CCR6A, MET, IL2RGA, TNFB, IL12RB2, IFNPHI1, VEGFC, IL20RA, CCL20A.3, IL10RB, LEPA, TNFRSF18, TNFRSF19, TGFB1A, NGFRB, IL22RA2, THPO	19	2.6	2.48E-04	0.285
KEGG_PATHWAY	dre04630:Jak-STAT signaling pathway	STAT1B, IL6ST, PIK3CD, IL2RGA, IRF9, IL12RB2, SI:RP71-17I16.5, IFNPHI1, IL20RA, IL10RB, LEPA, IL19L, SOCS3B, THPO, IL22RA2	15	3.1	2.67E-04	0.307
GOTERM_MF_DIRECT	GO:0008374~O-acyltransferase activity	SOAT2, LCAT, NAA40, MBOAT4, GPAT2, YKT6, GPAM	7	7.6	2.13E-04	0.324
UP_KEYWORDS	Signal	LTBP1, IL6ST, SI:CH73-181M17.1, LHCGR, PDGFBA, EPDL1, B2M, SI:CH211-222K6.3, OGN, DEFBL1, LCAT, CFH, ZGC:153932, ERAP2, SERPINH1A, LAMB1A, SOSTDC1B, SI:DKEY-4C23.5, CCL34A.3, PKHD1L1, SI:CH211-145B13.6, ALPI.2, ZGC:100868, VEGFC, NPC2, ZGC:162608, SI:CH211-125E6.11, TGFB1A, ADAMTS5, UGT5G2, ZGC:77929, SI:RP71-1G18.7, IL17C, GNAIA, TMEM123, SI:CH1073-155H21.1, SI:CH1073-126C3.2, ZGC:163079, FREM2A, ZGC:123297, ADGRE14, APOBB.1, CYP2R1, HSPA13, MHC1ZBA, SI:CH211-134A4.3, SI:DKEY-112E17.1, LXN, NITR1B, LY86, NPNT, ZGC:171509, TAS1R3, SI:DKEY-84K17.2, CCL20A.3, PDPK1A, SCPP8, USP11, PRSS35, MBLAC1, SI:CH211-39F2.3, AVP, GIP, JKAMP, CNPY2, P4HA1B, SI:DKEY-162H11.3, CA4B, IL20RA, NITR13, FKBP14, TOR1L1, WNT9A, GPHA2, SI:CH73-334D15.1, ZGC:172053, HYAL2A, SEMA3GA, TFA, IL10RB, PLA2G12A, PLA2G12B, SEMA3GB, LY75, SI:DKEY-193C22.2, IGF3, STAB2, CLEC11A, ZGC:55621, KHK, CRFB15, FBLN2, SI:CH73-380L10.2, PCMTL, IGFBP1B, SEMA3FB, SI:CH211-207N23.2, SI:CH211-132G1.1, CCL20B, SI:CH211-132G1.4, IL2RGA, DICP2.2, VIPR2, MMP2, LYGL1, PRF1.1, CCL39.6, SI:CH211-125E6.5, SI:CH73-256J6.4, SI:CH211-133H13.1, SPARCL2, FZD7B, SI:DKEY-192K22.2, EPHB4B, ZGC:111983, SI:DKEY-88N24.8, MFAP5, PLXNC1, IGFBP5B, CTSS2.2, CTSS2.1, ITGB5, SI:CH211-145C1.1, SI:DKEY-247K7.2, IFNPHI1, SI:CH73-330K17.3, ANGPTL3, LOXL3A, HAVCR1, GNRH2, MPEG1.2, SI:CH73-329N5.6, SI:DKEY-239B22.1, MET, ADGRG1, SI:CH73-196I15.3, SI:CH211-76M11.8, SI:DKEY-37G12.1, CXCL19, ADGRF8, ITGA8, SI:DKEY-21E2.8, SLC8A2A, PCOLCE2B, IL22RA2, ANTXR1D, GM2A, HEXA, HDR,	218	1.2	9.33E-04	1.178
GOTERM_CC_DIRECT	GO:0005615~extracellular space	SERPINB1L1, SI:DKEY-23A13.6, CCL20B, IGFBP5B, LUM, CTSS2.2, ZGC:154142, CTSS2.1, ZGC:171509, SEMA3AB, PDGFBA, IGF2A, IL17C, TNFB, OGN, IFNPHI1, SEMA3GA, TFA, WNT3, SI:CH211-113A14.19, CCL20A.3, LEPA, CECR1A, C18H3ORF33, SEMA3GB, DIA1B, SERPINH1A, SOSTDC1B, SAAL1, INHA, IGF3, VEGFC, SI:CH73-36P18.5, CPAMD8, CTSD, CTSC, SI:CH73-380L10.2, TGFB1A, IGFBP1B, SEMA3FB	40	1.7	0.001	1.531
GOTERM_MF_DIRECT	GO:0004888~transmembrane signaling receptor activity	LY75, OR132-4, ADGRF6, SI:CH211-282J17.8, OR111-11, OR104-2, FZD7B, VIPR2, ADGRG1, OR103-2, SI:CH211-218M3.18, SI:DKEY-83F18.7, SI:CH211-225K7.3, ADGRE16, ADGRF8, OR105-1, ADGRE14, SI:CH211-225K7.5, ADGRE5B.2, SI:DKEY-23C22.5, SI:DKEY-88N24.8, PLA2R1, SI:CH211-282J17.1, OR126-3	24	2.1	0.001	2.160
GOTERM_BP_DIRECT	GO:0051607~defense response to virus	MXF, IFNPHI1, BNIP3LA, IFIT14, MXC, SI:CH73-236C18.8, LY86, MXA	8	4.6	0.002	2.354
INTERPRO	IPR011029:Death-like domain	DLG5B.1, SI:CH211-114L13.9, IRAK3, CARD9, CASP9, SI:DKEY-103E21.5, HDR, SI:DKEY-61P9.9, SI:CH211-66K16.2, SI:DKEY-29H14.10, SI:CH211-171L17.4, ADGRG1, NGFRB	13	2.9	0.002	2.611
GOTERM_BP_DIRECT	GO:0019885~antigen processing and presentation of endogenous peptide antigen via MHC class I	ERAP1A, ERAP1B, ERAP2, TAPBPL	4	12.8	0.003	4.194

[a)] https://david.ncifcrf.gov

A)

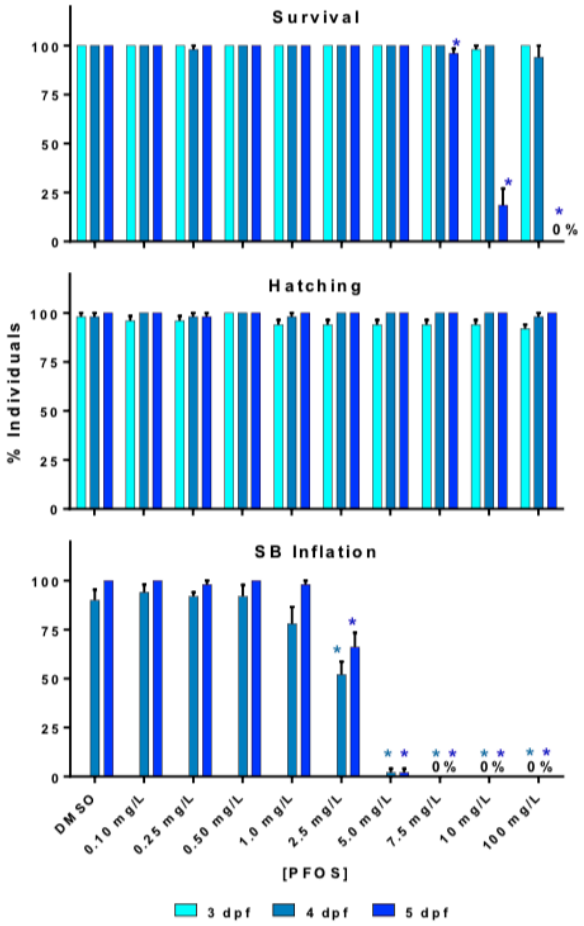
Survival
Hatching
SB Inflation
% Individuals
100
75
50
25
0
0 %
DMSO
0.10 mg/L
0.25 mg/L
0.50 mg/L
1.0 mg/L
2.5 mg/L
5.0 mg/L
7.5 mg/L
10 mg/L
100 mg/L
[PFOS]
3 dpf
4 dpf
5 dpf

B)

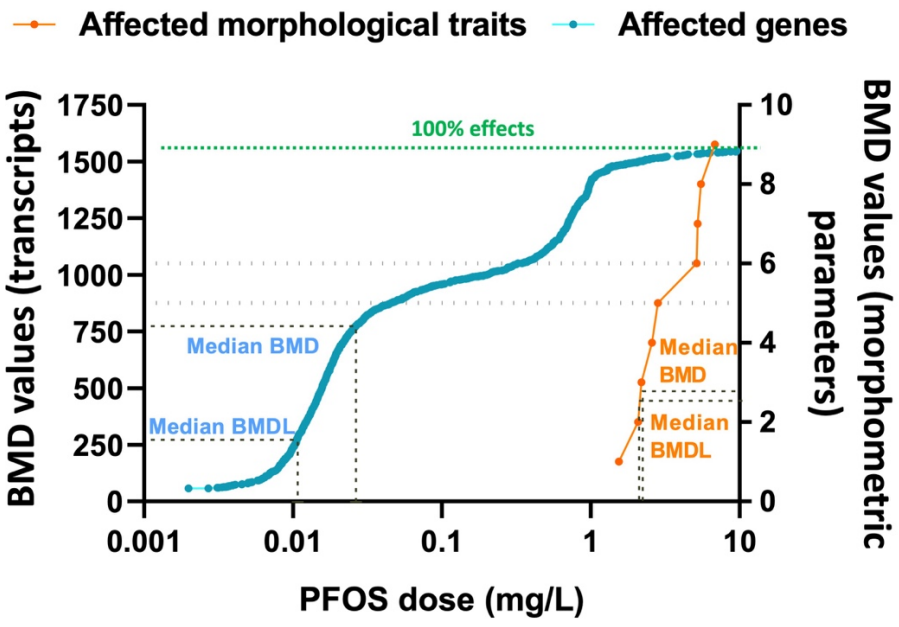
Affected morphological traits
Affected genes
100% effects
Median BMD
Median BMDL
Median BMD
Median BMDL
BMD values (transcripts)
BMD values (morphometric parameters)
PFOS dose (mg/L)
1750
1500
1250
1000
750
500
250
0
10
8
6
4
2
0
0.001
0.01
0.1
1
10

Supplementary Figure 1. **Quantitative analysis of survival, morphometric and transcriptional data. A)** Survival, hatching and swim bladder (SB) inflation rates of zebrafish embryos exposed to PFOS in the morphometric test. Measurements were taken at 3, 4 and 5 dpf. Bars represent the mean value ± SEM (standard error of the mean) for each group. Non-parametric test (Kruskal-Wallis with pairwise multiple comparisons, $p < 0.05$) was performed. Colored asterisks indicated statistical differences between exposed embryos and the corresponding control group for each age. **B)**. Benchmark dose (BMD) analysis for morphometric and transcriptional changes. The graph shows accumulation plots of the best calculated BMD for each gene and morphological trait. BMD was calculated for each parameter by the BMDExpress software (https://www.sciome.com/bmdexpress/), using a combination third-order polynomial, third-order exponential and Hill equations, and choosing the best fitted model for each case separately. In case of the genes, only those with more than 100 counts between all the 12 replicates and a fold change > 1.5 or <0.75 were used. The median values of BMD and BMDL were calculated as 0.027 and 0.011 mg/L for the transcriptomic effects and 2.83 and 2.53 mg/L for the morphological effects, respectively. BMDL values were considered as PoD (Point of Departure) levels, doses at which negative effects started being significant). Dotted lines indicate the range coincidence of transcriptomic and morphological effects (in terms of % of affected genes/traits) between the most and less sensitive parameters.

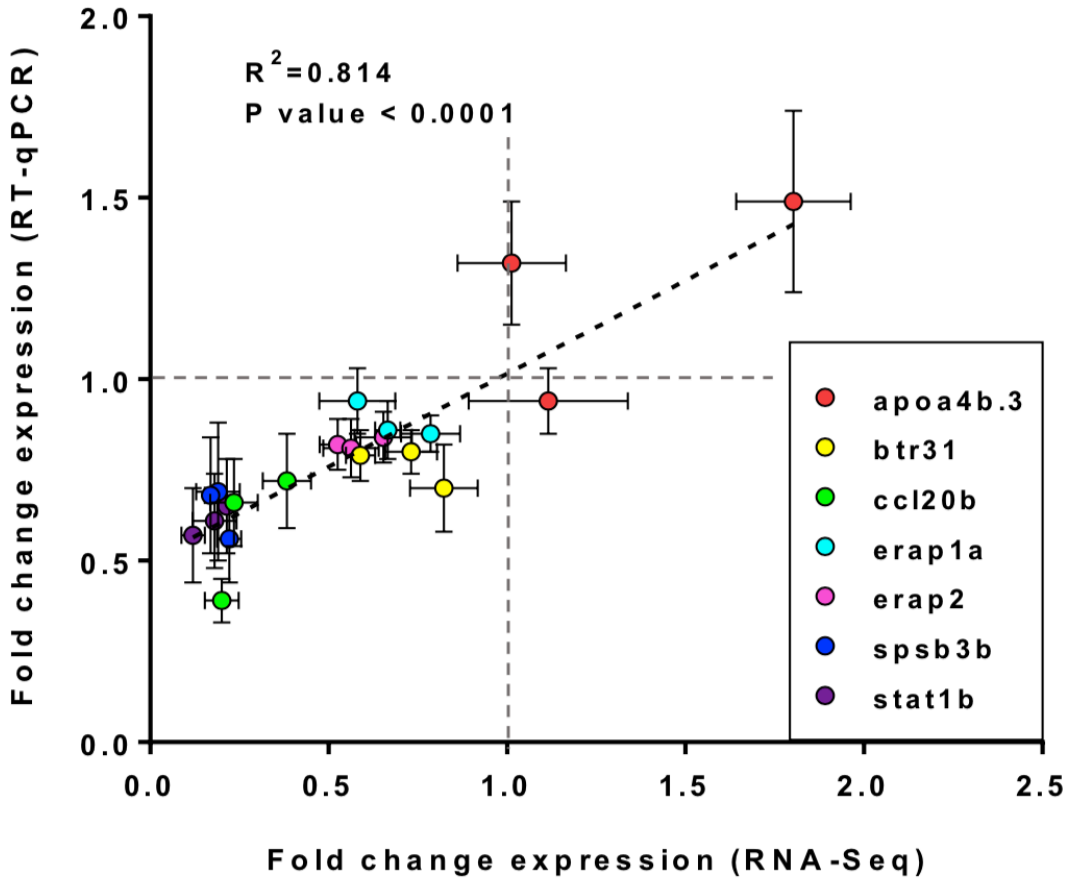

Supplementary Figure 2. Correlation between RNAs-Seq and RT-qPCR relative expression of some selected genes (apoa4b.3, btr31, ccl20b, erap1a, erap2, spsb3b and stat1b). Fold change expression data were used and a linear regression performed. Colored points represent the mean fold change ± SEM (standard error of the mean) of the three treatment groups (0.03, 0.3 and 1.0 mg/L of PFOS) per each gene. Three and nine replicates were used for RNA-Seq and RT-qPCR, respectively.

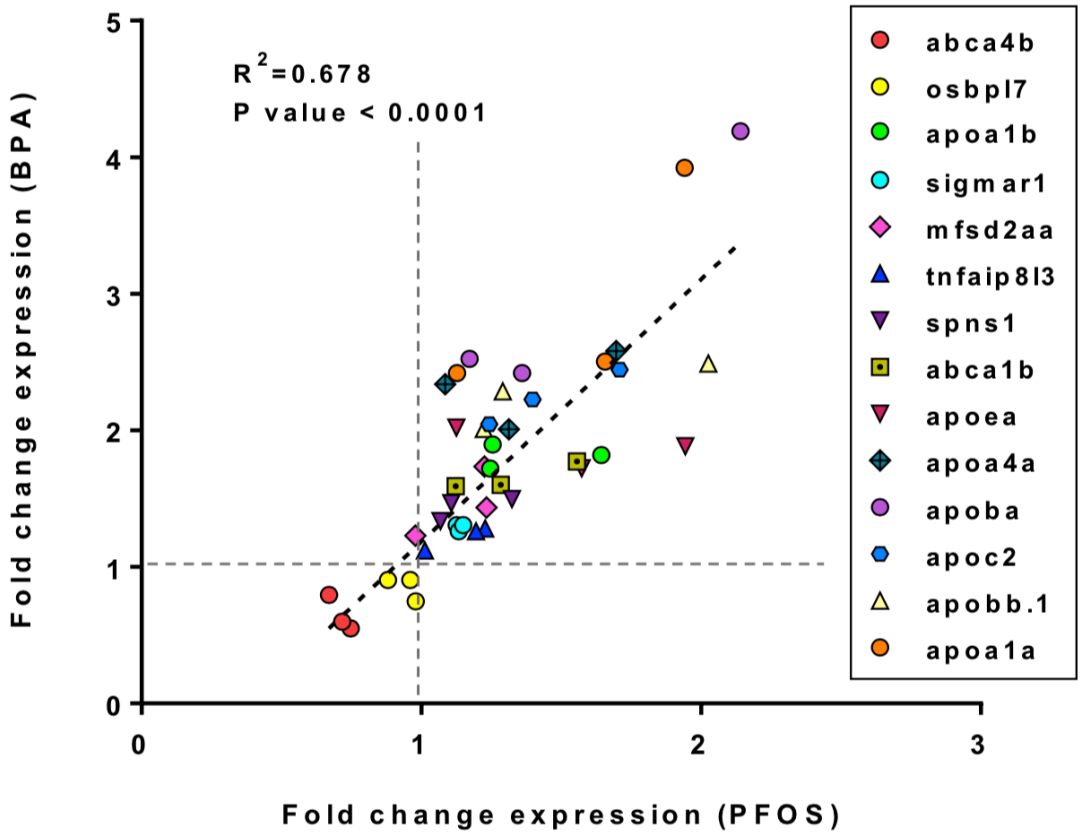

Supplementary Figure 3. Correlation of the relative expression (measured with RNA-Seq) of the differentially expressed genes (DEGs) related with lipid transport/metabolism between our PFOS exposure and a previous BPA exposure done in the same developmental timing and conditions [33]. For comparison, the most similar groups between exposures were linked with each other (controls between them -not used for the regression-, 1/40 LOAEC of BPA with 1/30 LOAEC of PFOS, 1/4 LOAEC of BPA with 1/3 LOAEC of PFOS and LOAEC of BPA with LOAEC of PFOS). Fold change expression data were used and a linear regression performed. Each point represents the mean value ± SEM (standard error of the mean) of the 3 transcriptomic replicates used in each exposure.

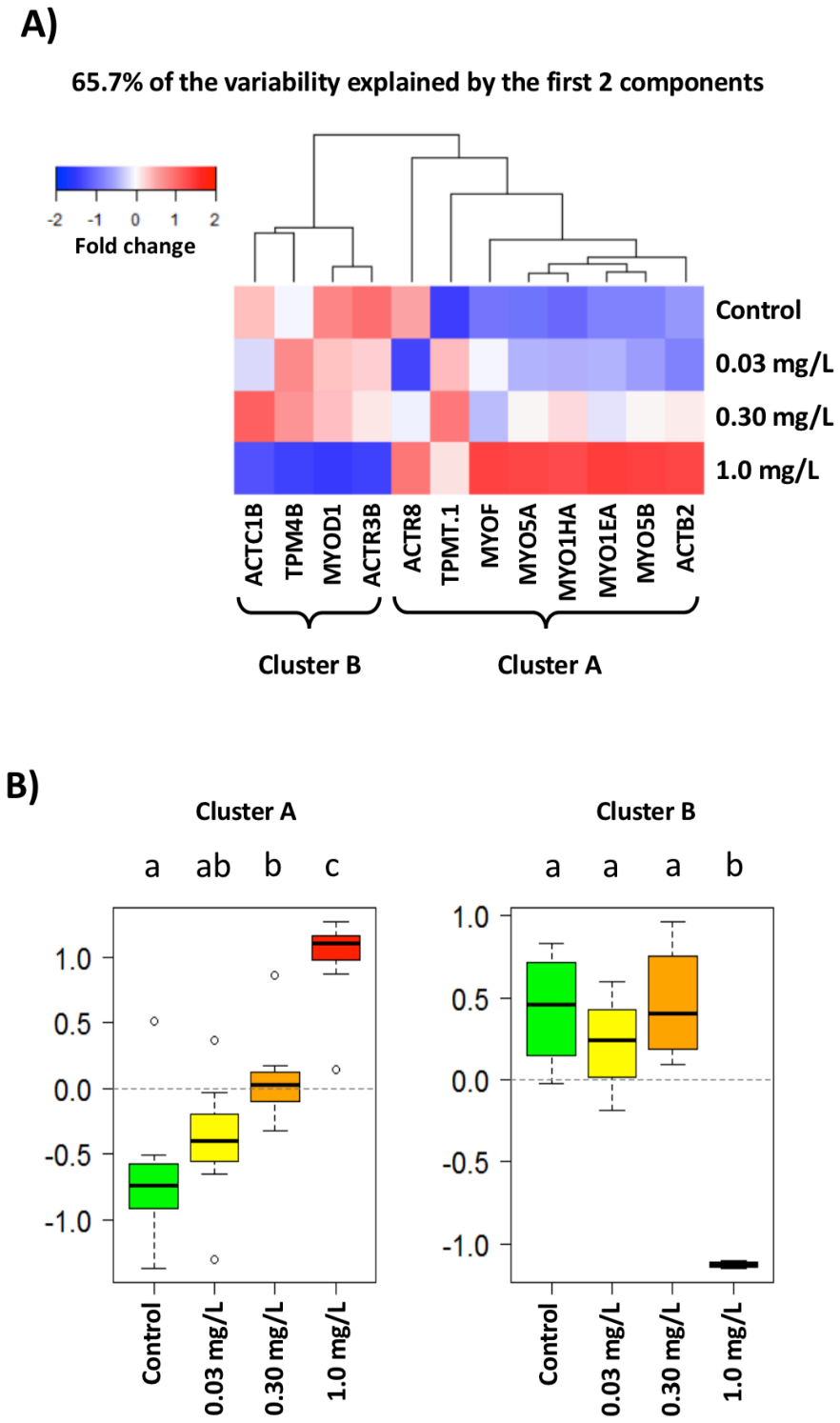

Supplementary Figure 4. Analyses of the myosines, tropomyosins and actins categorized as DEGs in the general transcriptomic analyses. A) Heatmap showing concentration changes corresponding to the 12 transcripts (only considering myosines, tropomyosins and actins) identified by ANOVA-PLS as differentially expressed genes (DEGs) in at least

one of the experimental groups. Values were centered to the average of control samples and log2 transformed. The mean value of the 3 replicates is shown for each group. Color scale ranges from blue (strongly underexpressed relative to control) to red (strongly overexpressed); white cells correspond to control values (fold change = 0). Rows (genes) were grouped by hierarchical clustering and its corresponding dendrogram is shown at the top of the panel. The two clusters (A and B) determined in a posterior medoids PAM clustering analysis are indicated. B) Normalized abundance values for all the genes included in each of the two clusters (cluster A at left, which contains the overexpressed genes due to PFOS exposure, and cluster B at right, which contains the underexpressed genes). Low-case letters at the top of each graph indicate statistically different distributions (parametric ANOVA + Tukey's B post-hoc test with all pairwise comparisons, $p \leq 0.05$). Boxes include values between the 1st and 3rd quartiles, thick bars indicate average values and whiskers cover the total distribution, except for outliers (circles).